Perturbation of boundary conditions to create appropriate ensembles for regional data assimilation in coastal estuary modeling

Yoshitaka Matsuzaki [1] and Tetsunori Inoue [1]

[1] Marine Environment Control System Department, Port and Airport Research Institute, Yokosuka, Japan

Corresponding author: Yoshitaka Matsuzaki (matsuzaki-y@p.mpat.go.jp)

Key Points:

- This is the first study to apply the ensemble Kalman filter to an actual coastal estuary using real one-year observation data
- It is possible to maintain the ensemble spread by perturbing atmospheric forcing, lateral boundary conditions, and river discharge forcing
- This method achieves robust annual data assimilation and reflects seasonal fluctuations

Abstract

Regional data assimilation is conducted for a coastal estuary using the ensemble Kalman filter, real observation data from Ise Bay, Japan, and a simulation model called the Ise Bay Simulator. The applicability and robustness of the method are then examined. We also analyze the relationship between the boundary conditions, which add perturbations and the data assimilation results of water temperature and salinity. A method of creating an ensemble by perturbing three boundary conditions (atmospheric forcing, lateral boundary conditions, river discharge forcing) is then proposed. In situ water temperature and salinity profiles observed at fixed points are assimilated daily. The proposed assimilation method provides stable data assimilation without unnatural values for water temperature and salinity throughout the year. Further, applying a perturbation to the three boundary conditions does not lead to filter divergence, thus indicating good applicability and robustness. Applying a perturbation to the three boundary conditions does not degenerate the ensemble spread. According to a sensitivity experiment, perturbing the atmospheric boundary conditions of air temperature and wind speed increases the ensemble spread of water temperature, especially near the surface layer. Wind speed has the greatest influence on the magnitude of the salinity ensemble spread, and its dominance depends on location. Perturbation of lateral boundary conditions increases the ensemble spread of water temperature and salinity at all water depths near the bay mouth, and the observations are effectively assimilated. Perturbation of river discharge forcing successfully assimilates water temperature and salinity near the estuary.

Plain Language Summary

The accuracy of numerical simulations of physical quantities such as water temperature and salinity in coastal estuaries may be hindered by limitations to set accurate calculation conditions. Therefore, data assimilation is used to integrate observed values into numerical simulations. However, despite progress in large-scale data assimilation (for example, in the open ocean), applying data assimilation to small-scale complex phenomena in coastal areas is lacking. In this study, we propose a data assimilation method for a coastal area; specifically, Ise Bay in Japan. For data assimilation, it is particularly important to set an appropriate coefficient (background error covariance) that determines how to incorporate the observed values into the numerical simulation. Among the various numerical simulation conditions, we hypothesize that the boundary conditions have a dominant effect on the error of the numerical simulation in coastal areas; therefore, we set the boundary conditions according to the magnitude of error. The data assimilation results for water temperature and salinity over one year exhibit high accuracy and verify the applicability and robustness of the proposed data assimilation method.

1 Introduction

There are certain difficulties in conducting precise numerical simulation of physical phenomena at coastal estuaries. Data assimilation methods can improve the reproduction accuracy and advance our understanding of physical processes. However, applying data assimilation to coastal numerical simulations is still challenging because of the complexity of the physical process (Stanev et al., 2016). One of the most important conditions of data assimilation is the background error covariance (forecast error covariance) (Edwards et al., 2015; Hoteit et al., 2018; Moore et al., 2011; Sakov et al., 2012). Although there are several methods for calculating

the background error covariance (Fisher & Courtier, 1995; Fu et al., 1993; Weaver & Courtier, 2001), an appropriate method for regional data assimilation in coastal estuaries has not yet been determined. From this viewpoint, the ensemble Kalman filter (EnKF), which can express and update the background error covariance using ensemble members that indicate the system error, i.e., the numerical simulation error (Evensen, 1994), is a potential procedure for coastal calculation.

Ensemble members are created by perturbing the error factors of numerical simulations to represent the ensemble spread or variability. There are approximately three types of error factor that contribute to the error of a numerical simulation: (1) initial conditions, (2) forcing data, and (3) model equations and parameters (Turner et al., 2008). For numerical models of open oceans, which are relatively advanced in data assimilation, several studies have suggested calculating ensembles to represent the atmospheric forcing errors (Lima et al., 2019; Mirouze & Storto, 2019; Penny et al., 2015; Sakov et al., 2012), parameter errors (Brankart et al., 2015), and their combinations (Baduru et al., 2019; Kwon et al., 2016; Sanikommu et al., 2020; Vandenbulcke & Barth, 2015). This reflects the assumption that initial conditions, models, and atmospheric boundary conditions are important for the precise simulation of physical processes in the open ocean, which has a relatively large calculation area and long-term fluctuations.

However, the successful perturbation of error factors to generate ensembles has not yet been achieved for regional data assimilation in coastal estuaries. We suggest that perturbation of three boundary conditions is required to generate ensembles for regional data assimilation of a coastal estuary specifically, atmospheric forcing, lateral boundary conditions, and river discharge forcing. This is because coastal areas are more affected by boundary conditions because of the small calculation area. Moreover, it is very difficult to set accurate boundary conditions because of limitations of available data set, despite their substantial influence on the results of regional coastal numerical simulations. Previous studies have reported that error variability caused by the initial conditions decreases with time in coastal numerical models (Turner et al., 2008) because such models are dominated by relatively short-term fluctuations. Moreover, the error caused by the initial conditions can be maintained by multiplicative inflation (Anderson & Anderson, 1999; Whitaker & Hamill, 2012); however, this technique does not generate a consistent physical model (Sanikommu et al., 2020).

Some previous studies have conducted regional data assimilation for coastal estuaries using EnKF. For example, Turner et al. (2008) generated ensemble members for EnKF by perturbing atmospheric forcing, lateral boundary conditions, and river discharge forcing. They also proposed adding random noise with a normal distribution to the boundary conditions of the ensemble members as a method of perturbation. They applied this method to observing system simulation experiments (OSSEs) in Port Phillip Bay, Australia, using assimilated sea surface temperature (SST) data modified for satellite observations, and reported good prediction capability. Hoffman et al. (2012) also conducted OSSEs in Chesapeake Bay, USA. The assimilated data included fixed point water temperature, salinity, and SST, modified from in situ and satellite observations. They created ensembles by perturbing the initial conditions and wind via atmospheric forcing. Although they did not add perturbations to lateral boundary conditions and river discharge forcing, they noted it may be necessary to add perturbations to lateral boundary conditions and river discharge forcing for generating ensembles when data assimilation is conducted using real observation data. Furthermore, Khanarmuei et al. (2021) conducted twin experiments and OSSEs for the shallow estuary of Currimundi Lake, Australia. They perturbed

the lateral boundary condition of water level and river discharge, forcing to assimilate the observed values of water level and current velocity. They also revealed the importance of the combined perturbation of boundary conditions and assimilated observations. Thus, it is important to perturb the lateral boundary condition of water level when assimilating the observed value of water level, and to perturb river discharge forcing when assimilating the observed value of current velocity. However, real observation data were not included in their experiments and synthetic observation data were simulated numerically. In addition, the error factors were already known because the experiments were virtual.

Thus, we conducted the EnKF in the Ise Bay, Japan (it is coastal area including estuary, and same target simulation area in this study) using actual observed data (Matsuzaki & Inoue, 2020). Ensembles were made to perturb lateral boundary condition of water temperature and river water temperature. The assimilation results were compared with the observed values, and it was confirmed that the water temperature improved. However, this study was conducted only in the summer, and the data assimilation performance and the robustness of the data assimilation method throughout the year have not been evaluated. Therefore, it is imperative to conduct assessment throughout the year to respond to seasonal fluctuations and confirm applicability and robustness of the methods (Turner et al., 2008).

In this study, we conduct regional data assimilation for a coastal estuary using real observation data from Ise Bay, Japan, and evaluate the applicability of the data assimilation method. Specifically, we analyze the optimal method for adding perturbations to create ensemble members for regional data assimilation of a coastal estuary. This study also analyzes the relationship between the boundary conditions, which add perturbations and the assimilated water temperature and salinity data results as well as their ensemble spread. To the best of our knowledge, this is the first study to employ EnKF with actual water temperature and salinity data for a coastal estuary over one year. Additionally, no previous studies have generated ensembles by perturbing lateral boundary conditions and river discharge forcing under practical conditions; thus, this study reveals the effect of perturbing boundary conditions. In addition, we confirm the robustness of the regional coastal data assimilation method by performing long-term integral data assimilation and quantitative evaluation using the data assimilation results. The proposed data assimilation method is characterized by high applicability to coastal estuaries and responds to both short-term and long-term fluctuations, including seasonal changes.

2 Materials and Methods

2.1 Simulation model and setup

Simulations were conducted using the Ise Bay Simulator (Tanaka & Suzuki, 2010), which is a non-hydrostatic numerical simulation model. The model was configured to cover the entire area of Ise Bay (Figure 1, surface area: 2,342 km^2, mean depth: 17 m, volume: 3.94×10^{10} m^3), which is located in the south-central part of Honshu Island, Japan. The bay is approximately 70 km long in both longitudinal and latitudinal directions and is divided into two. The western side has a surface area of 1,738 km^2, a mean depth of 20 m, and a volume of 3.39×10^{10} m^3. The eastern side is called Mikawa Bay, which has a surface area, mean depth, and volume of 604 km^2, 9 m, and 5.5×10^9 m^3, respectively. The lateral boundary borders the Pacific Ocean. The Ise Bay model uses the cartesian coordinate system, which simulates the water current structure of coastal estuaries with a high horizontal resolution of 800 m. The coordinate system is set by

rotating it counterclockwise by 45°. The number of vertical layers is 32, with 0.5-m spacing near the water surface and 30-m spacing near the seabed. Input water depth data were created by reading the water depth from a chart made by the Japan Coast Guard. A subgrid-scale model was used for the horizontal turbulence model; the model of Nakamura and Hayakawa (1991), which has been modified from the model of Henderson-Sellers (1985), was used for the vertical turbulence model. The Sommerfeld radiation condition was applied for the transmission condition of the lateral boundary (Orlanski, 1976).

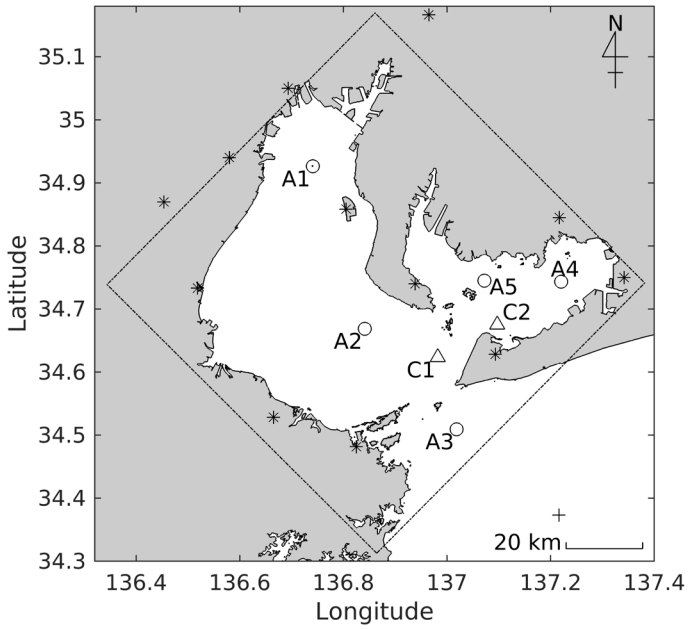

Figure 1. Location of Ise Bay, Japan. Dashed line indicates the experimental area for data assimilation. Circles and triangles represent observation stations used for data assimilation and accuracy validation, respectively. Asterisks represent the observation stations used to generate atmospheric forcing data. Crosses represent the observation points used to generate the lateral boundary conditions.

2.2 Boundary condition settings

This simulation system, which includes data assimilation, is designed from the perspective of short-term forecasts. Therefore, the data used for the boundary conditions were created using only data available in real time. Thus, more accurate data were not used for boundary conditions unless they could be obtained in real time. Thus, although a system that uses the output of an atmospheric simulation model as a boundary condition has since been developed for this numerical simulation model (Hafeez et al., 2021; Matsuzaki et al., 2021), this study adopted a system that creates boundary conditions based on observed values.

2.2.1 Atmospheric forcing

Atmospheric forcing data were generated from observation data from 12 terrestrial observation stations of the Automated Meteorological Data Acquisition System (AMeDAS) near Ise Bay (Nagoya, Centrair, Gamagori, Minamichita, Toyohashi, Irago, Kuwana, Yokkaichi, Kameyama, Tsu, Omata, and Toba). All atmospheric forcing data at each calculation grid were

interpolated using weighting interpolation with a normal distribution (the variance was 100 km^2) according to the distance from the observation stations. Shortwave radiation was calculated from daylight hours following the method of Nimiya et al. (1997). Longwave radiation was calculated according to the method of Nimiya et al. (1996). Wind velocity was set as follows. The observed wind speed was converted to wind speed at an altitude of 100 m using the logarithmic law in Equations (1) and (2):

$$W = \frac{U^*}{\kappa} \ln \frac{Z}{Z_0} \quad (1)$$

$$U^* = \frac{W_0 \cdot \kappa}{\ln \frac{h_m}{Z_0}} \quad (2)$$

where W is the converted wind speed, U^* is the friction speed, κ is the Kalman constant ($\kappa = 0.4$), Z is the height from the bottom, Z_0 is the roughness length, W_0 is the wind speed at the observation station, and h_m is the altitude of the wind anemometer. The roughness length at the sea surface was set to 0.001 m, and the roughness length at each observation station was set according to the work of Kuwagata and Kondo (1990). Wind velocity at each calculation grid was interpolated using the same method as that for other weather data. Then, the wind speed at an altitude of 10 m was obtained by Equation (1). Vapor pressure e [hPa] was calculated using Equation (3) and (4):

$$e = es \times U/100 \quad (3)$$

$$es = 6.112 \times exp\left(\frac{17.62T_a}{243.12+T_a}\right) \quad (4)$$

where es is the saturation vapor pressure [hPa], U is the relative humidity [%], and T_a [°C] is the air temperature. The parameter es was calculated using the method of the World Meteorological Organization (2008).

2.2.2 Lateral boundary condition

The average water temperature and salinity of each day of the year are calculated from monthly observation data (observation point number A10, latitude 34.37325, longitude 137.21583, measurement depth: 0, 10, 20, 30, 50, 75, 100, and 150 m below sea level) for 10 years (2004 to 2013) obtained by the Aichi Fisheries Research Institute. Their data were used to generate the lateral boundary conditions of water temperature and salinity. The observation data were uniformly interpolated in the horizontal direction, linearly interpolated in the vertical direction, and linearly interpolated in the time direction. The tide level for the lateral boundary conditions was estimated using the amplitude and phase of 14 major tide components (Sa, Ssa, Mm, MSf, Mf, Q1, O1, P1, S1, K1, N2, M2, S2, K2) obtained from observation data of the Akabane tide station (latitude 34.6, longitude 137.18333) located near the lateral boundary. The estimated tide level was corrected using the atmospheric pressure.

2.2.3 River discharge forcing

The river discharge was calculated by a storage function method, as follows.

$$\frac{ds}{dt} = q_{up}(t) + r(t) - q(t) - q_{base} \quad (5)$$

$$s = k_1 q^p + k_2 \frac{dq}{dt} \quad (6)$$

$$Q(t) = \frac{q(t)}{3.6} A \quad (7)$$

where s is the apparent storage height of the basin [mm], t is time [h], r is the average precipitation in the basin [mm h^{-1}], q is the runoff over time t [mm h^{-1}], q_{up} is the runoff from the upper area [mm h^{-1}], q_{base} is the base runoff [mm h^{-1}], k_1, k_2, and p are constant values, Q is the

river discharge [m^3 s^{-1}], and A is the basin area [km^2]. Equation (6) is based on Prasad (1967). For the class A river in the basin, k_1, k_2, and p were obtained to compare the observed river discharge values. For other smaller rivers, few river discharge observations are made during precipitation events; therefore, the parameters were estimated using the average precipitation value in the basin multiplied by the basin area to obtain the river discharge. The average precipitation (r) in each basin was calculated as follows. Each river basin was divided into a grid. The distance between each grid point and the AMeDAS observation point was calculated, and any AMeDAS data point less than 30 km from a grid point was extracted. Here, the maximum number of AMeDAS observation points used at each grid point was 10. Precipitation at each grid was calculated by weighting according to the same method used for other weather data. The sum of precipitation for each grid was taken as the average precipitation of the basin.

River water temperature was calculated from the air temperature near the mouth of the river using Eq. (8):

$$T_w = aT_a + b \tag{8}$$

where T_w [°C] is the river water temperature, and a and b are parameters calculated from the relationship between the observed air temperature near the river mouth and the observed river water temperature.

2.3 Assimilation model

The EnKF model for the Ise Bay Simulator was coded (Matsuzaki & Inoue, 2020) based on the work of Evensen (2003). The settings for the ensemble simulation were the same as those described in section 2.1, and a novel data assimilation method with a high-resolution horizontal grid size (800 m) was employed. EnKF was implemented with 32 members. The ensemble number was chosen by referring to a previous study (Matsuzaki & Inoue, 2020). The observation data described below were assimilated once per day at 00:00. No localization technique was applied (Evensen, 2009; Gaspari & Cohn, 1999; Hamill et al., 2001); thus, it was possible to correct the entire Ise Bay based on the background error covariance using a physical model, instead of non-physical techniques such as the distance function. The multiplicative inflation technique was not applied because multiplicative inflation generates artificial vertical background error covariance (Sanikommu et al., 2020). Moreover, correlation of the observation error was ignored, i.e., the observation error covariance matrix was set to diagonal. As explained in section 2.4, perturbations were added to the boundary conditions to represent the system error. When assimilation was performed near the lateral boundary, the assimilation system became unstable. To stabilize the data assimilation, the two meshes adjacent to the lateral boundary were excluded from the assimilation, which ensured stable data assimilation performance.

2.4 Method of adding perturbations to boundary conditions

Generating a perturbation and determining its magnitude is a challenging task. Previous research has employed various methods to determine the boundary conditions for expressing an ensemble containing system noise, e.g.: (i) a method of adding noise according to a normal distribution (Turner et al., 2008), (ii) a method of adding red noise (Evensen, 2003; Sakov et al., 2012), (iii) a method of using ensemble simulation results (Bougeault et al., 2010) as the boundary condition (Sanikommu et al., 2020), and (iv) a method that considers the difference in state quantities at different times as a perturbation (Kunii & Miyoshi, 2012). This study employed method (i), as shown in Equation (9), because it was previously used to conduct

successful data assimilation for a coastal estuary; however, the study of Turner et al. (2008) employed OSSE instead of real data.

$$\boldsymbol{F_{mem}} = \boldsymbol{F_{base}} + \boldsymbol{v} \tag{9}$$

Here, $\boldsymbol{F}_{mem}$ indicates the boundary conditions for data assimilation with perturbation, F_{base} indicates the boundary conditions for numerical simulation, and $\boldsymbol{v}$ indicates the perturbations that have a normal distribution with a mean of zero and variance of ξ^2. For some boundary conditions, such as that shown in Equation (9), the additive method is not valid. For example, the boundary condition of river discharge may have a negative value when the river discharge is close to zero and noise with a normal distribution is added. In addition, when river discharge is larger, the error of river discharge forcing appears to increase. Thus, the following multiplication method was introduced:

$$\boldsymbol{F_{mem}} = \boldsymbol{v}\boldsymbol{F_{base}} \tag{10}$$

The model outputs evaluated in this study, which are explained in section 2.7, are water temperature and salinity. The boundary conditions considered having a large effect on the simulation error of water temperature and salinity were selected as follows. For the numerical simulation model, the atmospheric forcing boundary conditions include air temperature, shortwave radiation, longwave radiation, atmospheric pressure, wind direction, wind speed, water vapor pressure, and precipitation. The lateral boundary conditions include water temperature, salinity, and water level. The river discharge forcing boundary conditions include river discharge and river water temperature. Of these, the errors in the boundary conditions of air temperature, shortwave radiation, longwave radiation, lateral boundary water temperature, and river water temperature were considered directly linked to the numerical simulation error of water temperature. Similarly, the errors in the boundary conditions of precipitation, lateral boundary salinity, and river discharge were considered directly linked to the numerical simulation error of salinity. In addition, as water temperature and salinity are advected and diffused by the flow of water mass, the errors in the boundary conditions of wind speed, atmospheric pressure, and tide level of the lateral boundary were also considered having an effect. For these boundary conditions, these three assumptions were set. First, the shortwave radiation and longwave radiation errors were included in the air temperature error. Second, the precipitation error was included in the river discharge error. Third, the influence of the error between the atmospheric pressure and the tide level of the lateral boundary was relatively small, so was ignored. Therefore, the perturbations for atmospheric forcing were air temperature and wind speed, the perturbations for lateral boundary conditions were water temperature and salinity, and the perturbations for river discharge forcing were river discharge and river water temperature.

As the magnitude of the error is considered to correlate with the accuracy of the boundary conditions, the magnitude of the perturbation, ξ, for creating the ensemble must be determined by the same method used to generate the boundary conditions. In this study, ξ values were estimated according to the assumption that all calculated error distributions follow a normal distribution; ξ values calculated on a trial basis are shown in *Appendix A* and summarized in **Table 1**. When the normal distribution is expressed by a normal random number with a few members, there is the potential for a large deviation from the normal distribution due to sampling error. In this study, we did not use normal random numbers, but set the value of each member to

match the cumulative value of the normal distribution so the normal distribution can be expressed even with a few members. To avoid unintended correlation of each boundary condition, the Fisher-Yates shuffle (Fisher & Yates, 1948) was used to perform 10,000 replacement attempts, and the boundary conditions were set for each ensemble member using the combination with the lowest correlation.

Table 1. Magnitude of perturbations to boundary conditions. Calculation of ξ values is shown in Appendix A.

Boundary condition		Method	ξ
Atmospheric forcing	Air temperature	Equation (9)	3.04 °C
	Wind speed	Equation (9)	3.45 m s^{-1}
Lateral boundary conditions	Water temperature	Equation (9)	0.73 °C
	Salinity	Equation (9)	0.20
River discharge forcing	River discharge	Equation (10)	0.35
	River water temperature	Equation (9)	1.21 °C

2.5 Assimilated observations

In situ water temperature and salinity profiles observed at fixed points were used for the data assimilation. Seven in situ observation stations are in operation in Ise Bay. Data from the five observation stations in **Table 2** were assimilated. Observation error variance values were set to $(1.0\ °C)^2$ for water temperature and $(1.0)^2$ for salinity. These values were set referring to a previous study (Matsuzaki & Inoue, 2020). Gross error check was performed as background quality control. The difference between the observed value and the first guess value was calculated, and if the difference was over 3 °C for water temperature, and 6 for salinity; the observed value was rejected.

Table 2. Assimilated observation data.

No.	Station name	Latitude (ºN)	Longitude (ºE)	Observation type	Observation depth [m]
A1	Back of Ise Bay	34.926	136.741	Automatic elevating	Every 1.0 m
A2	Center of Ise Bay	34.669	136.841	Automatic elevating	Every 1.0 m
A3	Mouth of Ise Bay	34.509	137.018	Fixed	1.0 m, 11.8 m, and 23.2 m from low water level
A4	No. 1 buoy	34.743	137.220	Automatic elevating	Every 1.0 m
A5	No. 2 buoy	34.745	137.072	Automatic elevating	Every 1.0 m

320 ## 2.6 Experimental setup

321 Experiments were conducted for six cases (**Table 3**). In the standard experiment (case 1),
322 data assimilation was not applied, i.e., case 1 was a normal numerical simulation. Case 2
323 included the optimal settings determined before the experiment. Perturbations were applied to
324 three boundary conditions: atmospheric forcing, lateral boundary conditions, and river discharge
325 forcing. Cases 3–6 included the assimilation results but used different methods of generating the
326 ensembles. These experiments were conducted to confirm the effect of adding perturbations to
327 the boundary conditions by comparing the results with those of case 2. Case 3 had the same
328 conditions as case 2 but did not perturb the atmospheric forcing of air temperature and wind
329 speed, it analyzed the effect of considering the uncertainty of atmospheric forcing on the data
330 assimilation results. As case 4 applied perturbations to air temperature but not to wind speed, it
331 isolated the effects of air temperature and wind speed among the atmospheric forcing boundary
332 conditions. Finally, as cases 5 and 6 had the same conditions as case 2 but did not perturb the
333 lateral boundary conditions (case 5) or river discharge forcing (case 6), these experiments
334 examined the effect of considering the uncertainty of lateral boundary conditions and river
335 discharge forcing on the data assimilation results. The assimilation experiments were conducted
336 for one year from 1 January 2016, to evaluate the applicability of the proposed method to long-
337 term fluctuations, including seasonal changes, and to verify the robustness of the data
338 assimilation method. Initial ensembles for the assimilation experiments on 1 January 2016 were
339 generated using an eight-month spin-up period from 1 April 2015. Still, in the spin-up period, the
340 ensemble members were calculated under the boundary conditions including the perturbations,
341 and exhibited an ensemble spread according to the position and magnitude of the perturbation of
342 the initial conditions.

343 **Table 3.** Experimental conditions.

Experiment	Assimilation	Atmospheric forcing		Lateral boundary condition	River discharge forcing
		Air temperature	Wind speed		
Case 1	Control run without DA	NA	NA	NA	NA
Case 2	Assimilated	Perturbed	Perturbed	Perturbed	Perturbed
Case 3	Assimilated	Not perturbed	Not perturbed	Perturbed	Perturbed
Case 4	Assimilated	Perturbed	Not perturbed	Perturbed	Perturbed
Case 5	Assimilated	Perturbed	Perturbed	Not perturbed	Perturbed
Case 6	Assimilated	Perturbed	Perturbed	Perturbed	Not perturbed

344 ## 2.7 Accuracy validation

345 Water temperature and salinity data of the model output were compared with the in situ
346 observation data of water temperature and salinity profiles observed at fixed points (**Table 4**). As
347 it was impossible to prepare observation values such as SST for salinity, the model outputs and
348 data used for the assimilation (**Table 2**) were compared to evaluate and discuss the effects of
349 perturbing boundary conditions to generate ensembles. Observation data were collected every
350 hour, but the assimilations were conducted every day; thus, comparisons were conducted every
351 day. Water temperature data of the model output were also compared with the SST data observed
352 by Terra and Aqua (Moderate Resolution Imaging Spectroradiometer: MODIS) to evaluate the
353 correction of water temperature in the spatial direction. The MODIS SST data were obtained by
354 assuming that all data observed between 22:00 and 02:00 were observed at midnight; the SST

355 data were then compared with model output data for assimilation. The reproducibility of the
356 planar distribution of water temperature was then discussed.

357 **Table 4.** Comparison observation data not assimilated.

No.	Station name	Latitude (ºN)	Longitude (ºE)	Observation type	Observation depth
C1	Nakayama Channel	34.623	136.982	Fixed	1.4 m, 8.2 m, 12.4 m from low water level
C2	No. 3 buoy	34.675	137.097	Automatic elevating	Every 1.0 m

358

359 The accuracy of the model output was evaluated using two indices: the bias (Equation 10)
360 and the root-mean-square error (RMSE, Equation 11):

361 $$bias = \frac{1}{N}\sum_{i=1}^{N} e_i \quad (10)$$

362 $$RMSE = \sqrt{\frac{1}{N}\sum_{i=1}^{N} e_i^2} \quad (11)$$

363 where e_i is the simulation error (model output minus observation) and N is the number of model
364 outputs and observations. As degeneration of the ensemble spread becomes a problem when
365 executing EnKF (termed as filter divergence), the magnitude of the ensemble spread was
366 evaluated (Equation 12):

367 $$Ensemble\ spread = \sqrt{\frac{1}{mem-1}\sum_{i=1}^{mem}(x_i - \bar{x})^2} \quad (12)$$

368 where *mem* is the number of ensemble members (*mem* equals 32), x is a variable, and $\bar{\boldsymbol{x}}$ is the
369 average value of x.

370 **3 Results**

371 3.1 Performance and robustness of data assimilation

372 In this section, the results of the control run (case 1) and data assimilation (case 2) are
373 compared to show the validity and effectiveness of the data assimilation method. Figure 2 and
374 Figure 3 compare the time series of observed water temperature data in Nakayama Channel and
375 at the No. 3 buoy (Table 4) and the model output of case 1 and case 2. Case 1 exhibits the same
376 water temperature fluctuation trend as the observed values; however, the water temperature is
377 higher than the observed values. This difference is particularly large in the lower layer. Case 2
378 shows the water temperature corrected to match the observations. Moreover, case 2 was possible
379 to carry out the data assimilation for one year without breaking the calculation. Figure **4** and
380 Figure 5 show the biases and RMSEs between the observed and simulated water temperatures for
381 Nakayama Channel and the No. 3 buoy. Bias and RMSE values are lower for case 2 than case 1
382 at all depths. The bias improvement is approximately the same near the water surface and near
383 the bottom, with an average difference between case 1 and case 2 of 0.78 °C for Nakayama
384 Channel and 1.09 °C for the No.3 buoy. Conversely, the RMSE improvement is greater near the

bottom than near the sea surface. The average difference between case 1 and case 2 is 0.57 °C for Nakayama Channel and 0.86 °C for the No.3 buoy. These results indicate that the proposed regional data assimilation method for a coastal estuary is effective for correcting water temperature and highly robust, i.e., it can be applied throughout the year and reflects seasonal variations.

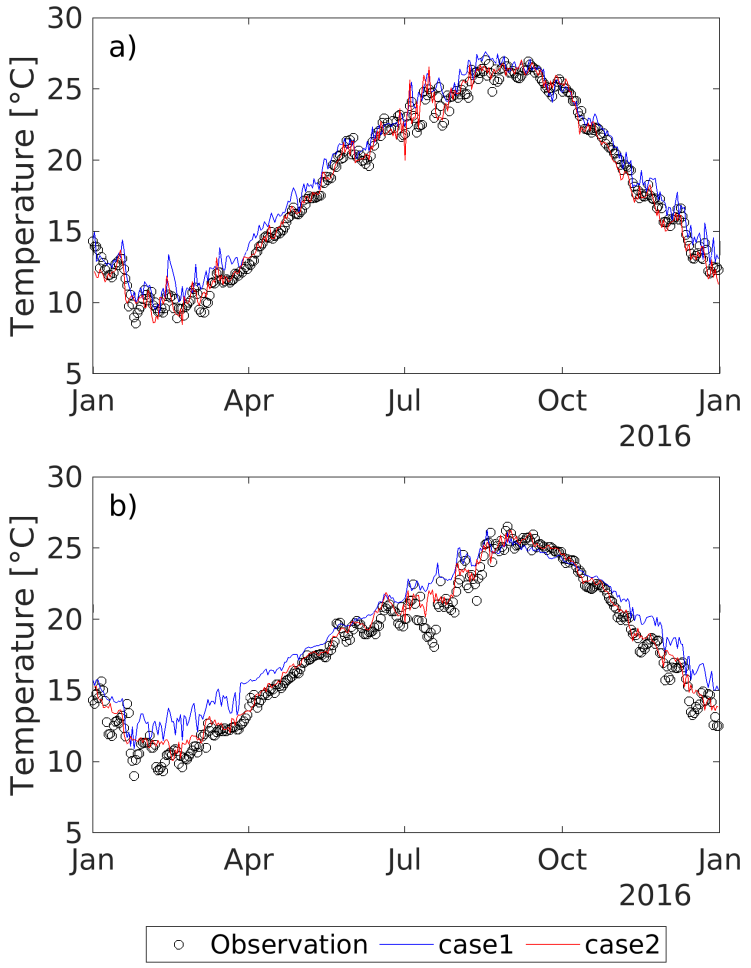

Figure 2. Timeseries of water temperature data at Nakayama Channel for observations, case 1, and case 2. a) water depth of 1.0 m; b) water depth of 12.0 m.

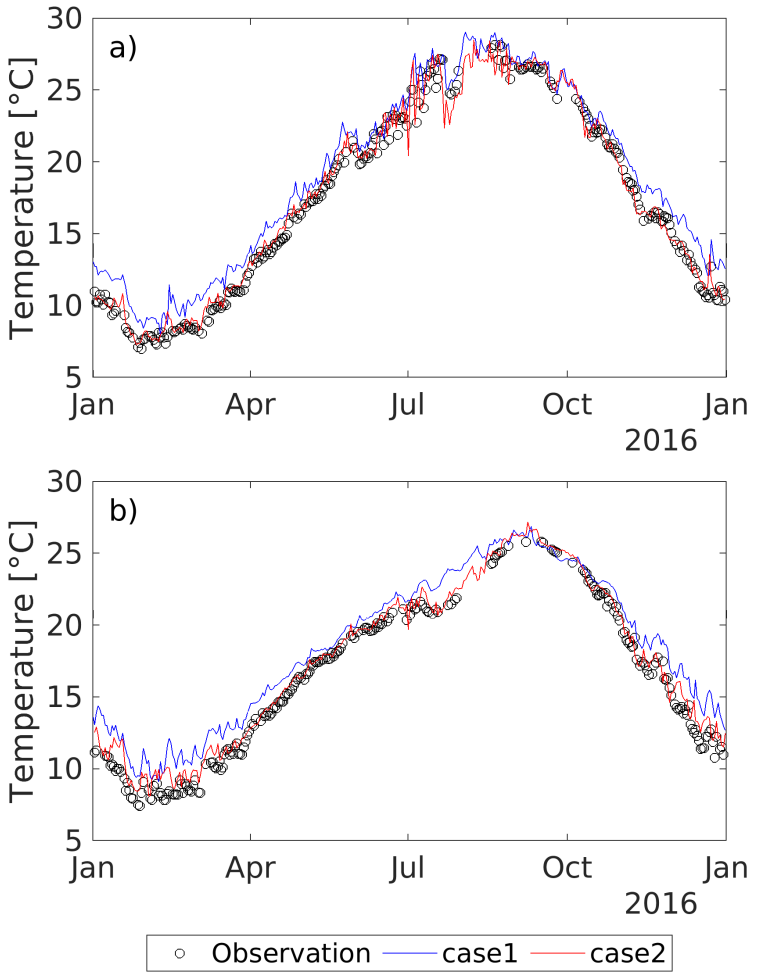

Figure 3. Timeseries of water temperature data at the No.3 buoy for observations, case 1, and case 2. a) water depth of 1.0 m; b) water depth of 12.0 m.

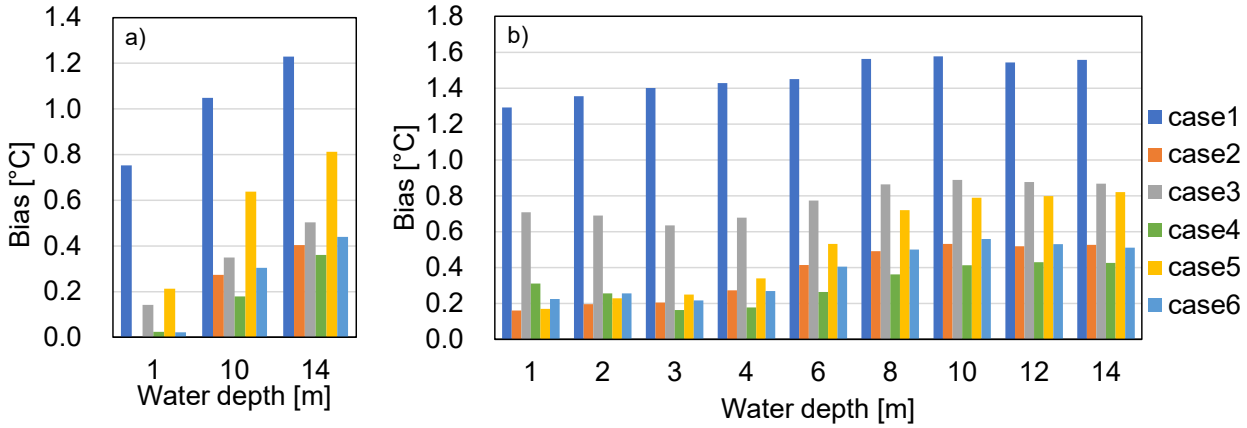

Figure 4. Bias between observed and modeled water temperature for all experiments. a) Nakayama Channel; b) No.3 buoy.

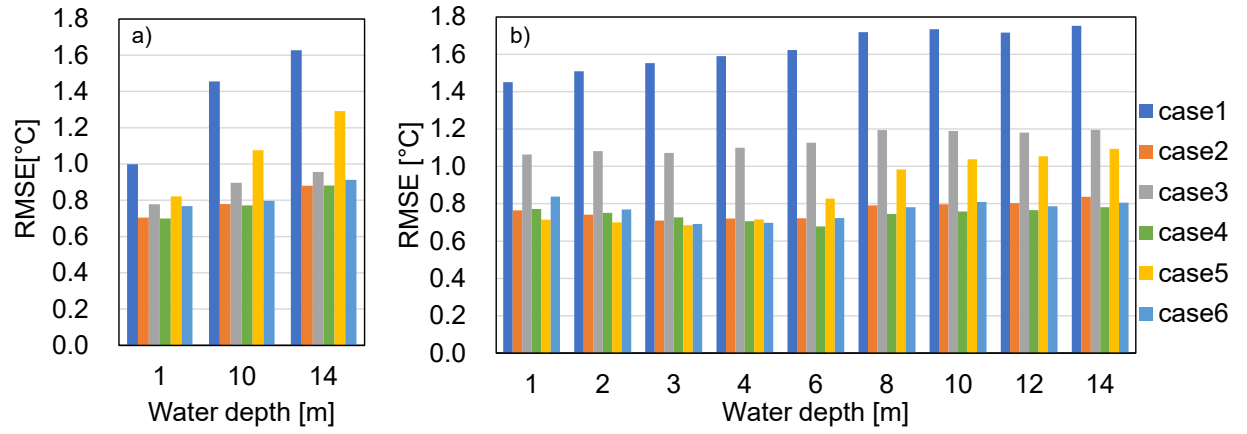

Figure 5. RMSE between observed and modeled water temperature for all experiments. a) Nakayama Channel; b) No.3 buoy.

Figure 6 and Figure 7 show the spatial distributions of bias and RMSE values between SST data observed by MODIS and the model outputs. The bias and RMSE values of case 2 data are lower than those of case 1 throughout Ise Bay, particularly at the west side of the bay, although the observed values used for data assimilation extend from the center of the bay to the east side, and there are no observation points on the west side. Data assimilation corrects the water temperature for the entire bay, despite sparse observations in the horizontal direction, because the error covariance is properly expressed by the proposed perturbation. Moreover, the bias and RMSE values of SST are 0.67 °C and 0.52 °C lower, respectively, in case 2 (Figure 8). Nevertheless, the bias and RMSE values do not exhibit substantial improvement on the east side of the bay mouth and in parts of the back of the bay. Thus, there is still room for further improvement.

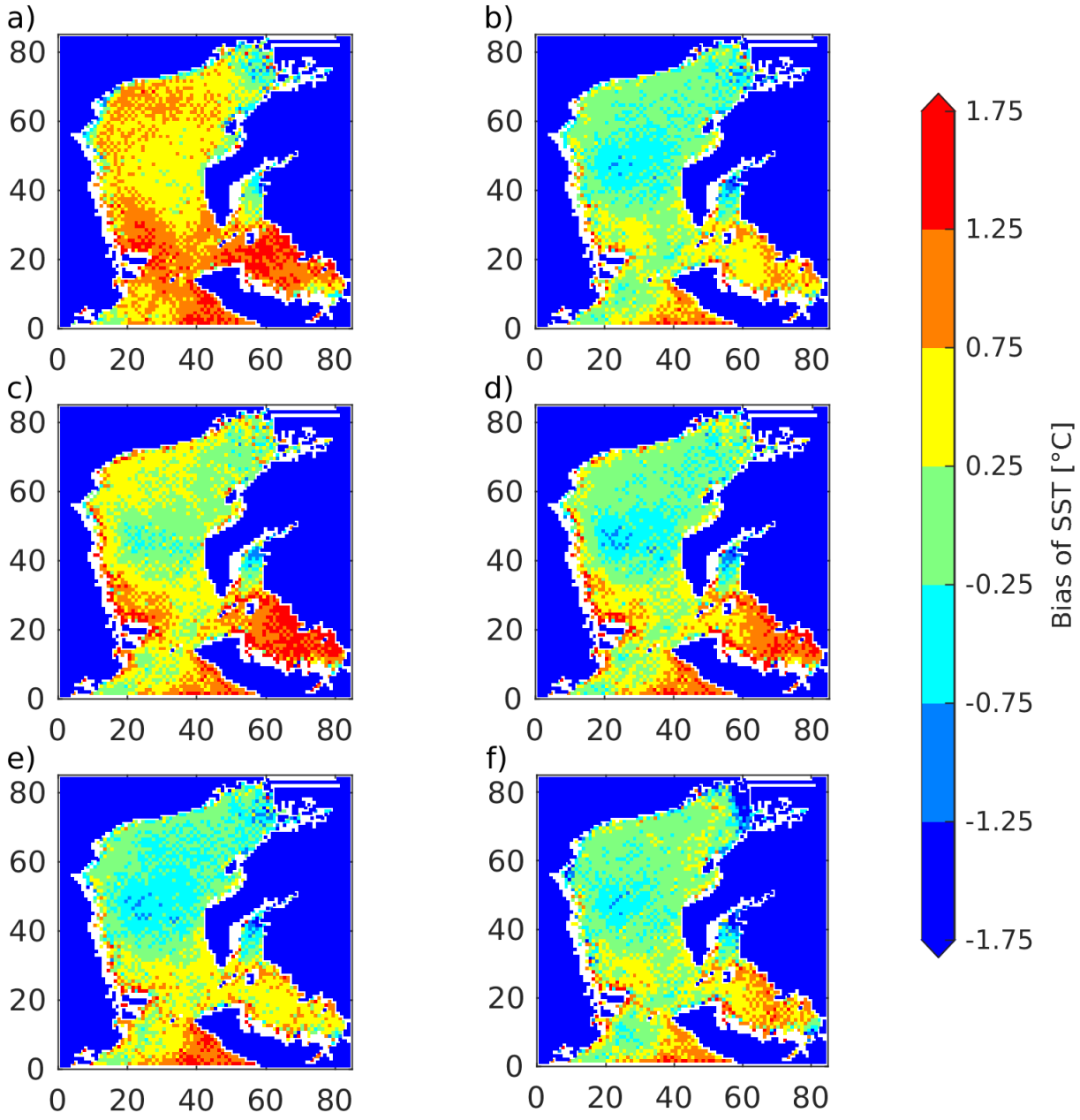

417

418 **Figure 6.** Planar images of the SST bias for a) case 1, b) case 2, c) case 3, d) case 4, e) case 5,
419 and (f) case 6. The horizontal and vertical axes indicate a calculation grid of 85 × 85.
420

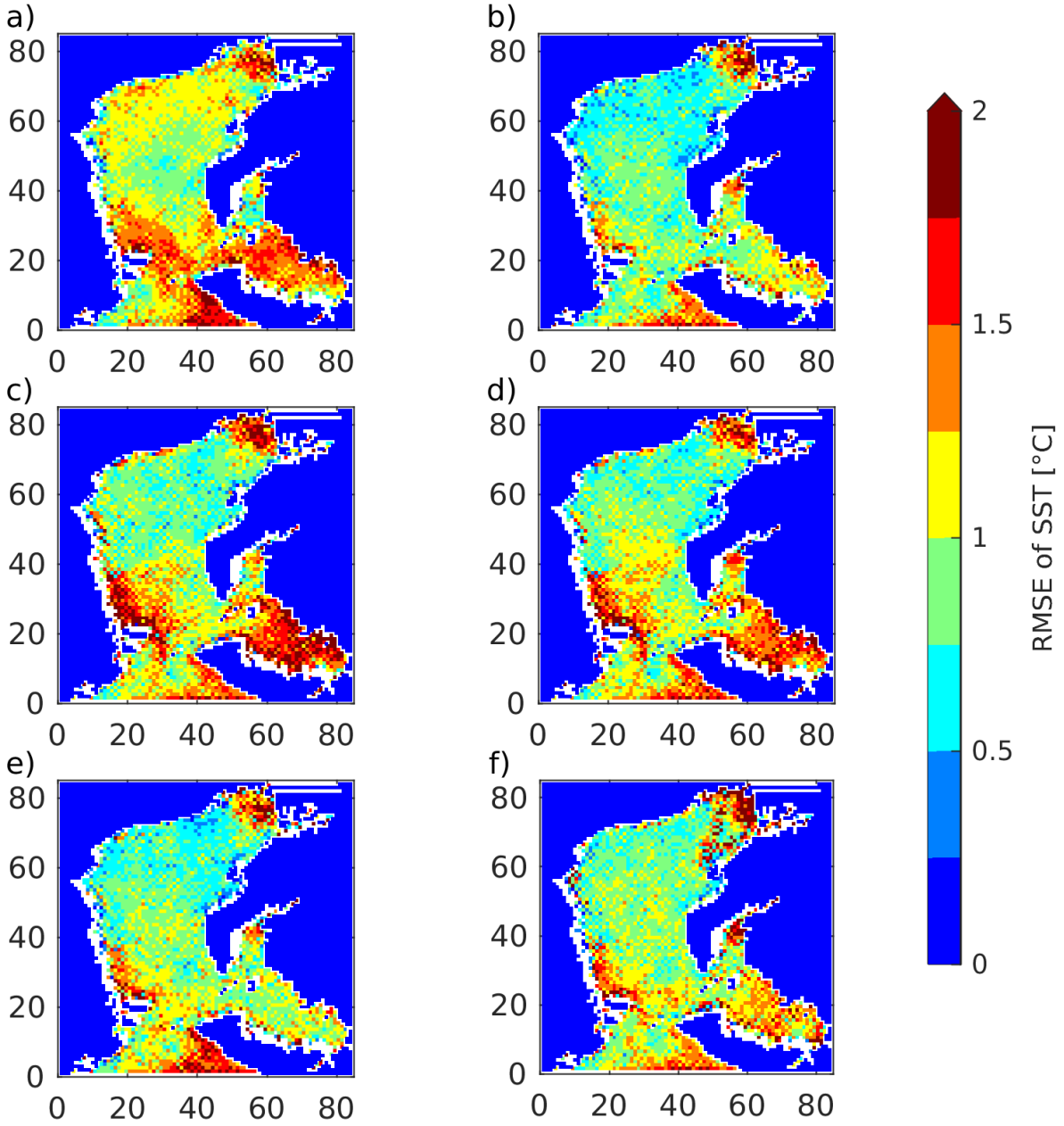

Figure 7. Planar images of the RMSE values of SST for a) case 1, b) case 2, c) case 3, d) case 4, e) case 5, and (f) case 6. The horizontal and vertical axes indicate a calculation grid of 85 × 85.

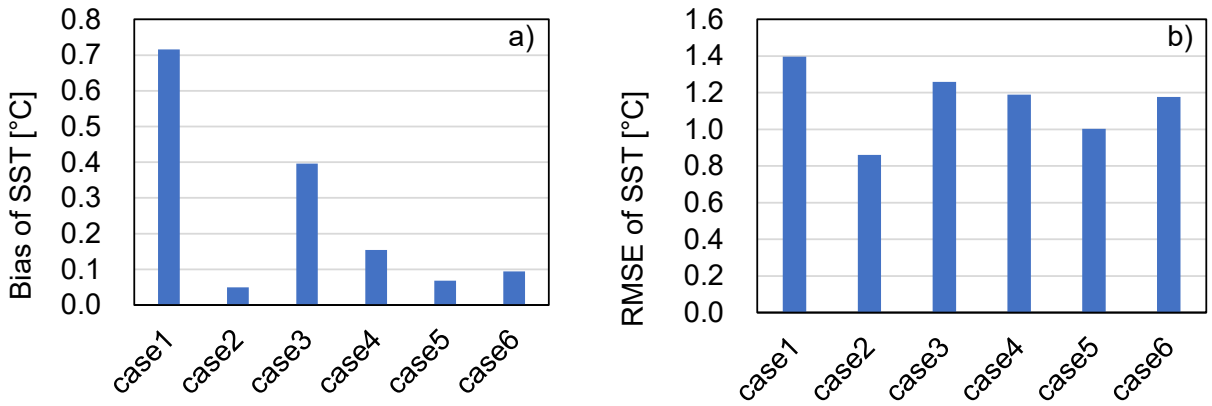

Figure 8. a) Bias and b) RMSE values of SST for all experiments.

Figure 9 and Figure 10 show time series of the observed salinity in Nakayama Channel and at the No. 3 buoy and the model outputs of case 1 and case 2. Although the effect of assimilation on salinity is not as clear as that for water temperature, the assimilation performance is stable throughout the year. Figure 11 and Figure **12** show the bias and RMSE values of salinity in Nakayama Channel and at the No. 3 buoy. Bias and RMSE values decrease from case 1 to case 2 at all depths in Nakayama Channel. The average difference in bias and RMSE values between the two experiments are 0.17 and 0.06, respectively. At the No. 3 buoy, the bias values are lower at all depths in case 2; however, the RMSE values do not show this trend; the average difference in bias and RMSE values between the two experiments are 0.07 and -0.09, respectively. One reason for this finding could be that the magnitude of perturbations (ξ) for assimilation of salinity data was not appropriate in the boundary conditions. When data assimilation is performed by only changing the magnitude of the perturbation of the boundary conditions from case 2 (the results of the sensitivity experiments are not shown, but ξ was set to 1.00 °C for air temperature, 2.00 m s^{-1} for wind speed, 0.50 °C and 0.25 for water temperature and salinity of the lateral boundary, 0.36 for river discharge, and 0.50 °C for river water temperature), the average RMSE of salinity at the No. 3 buoy is 0.01 smaller for case 2 than case 1. Therefore, the optimal magnitude of perturbation should be carefully considered. Nevertheless, the results indicate that the proposed regional data assimilation method for coastal estuaries is an effective and robust method for both water temperature and salinity data.

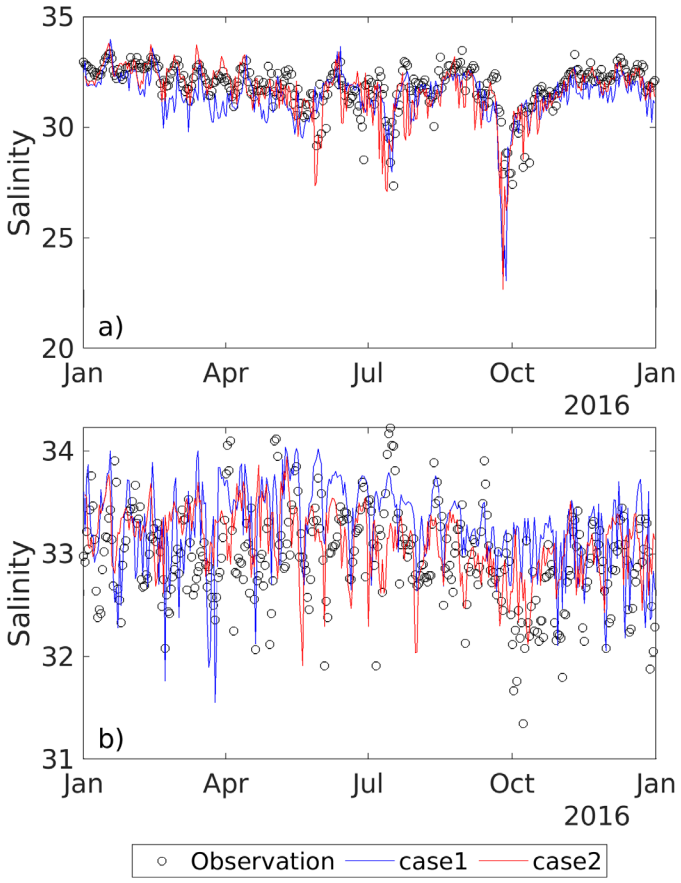

Figure 9. Timeseries of salinity at Nakayama Channel for observations, case 1, and case 2. a) water depth at 1.0 m; b) water depth at 12.0 m.

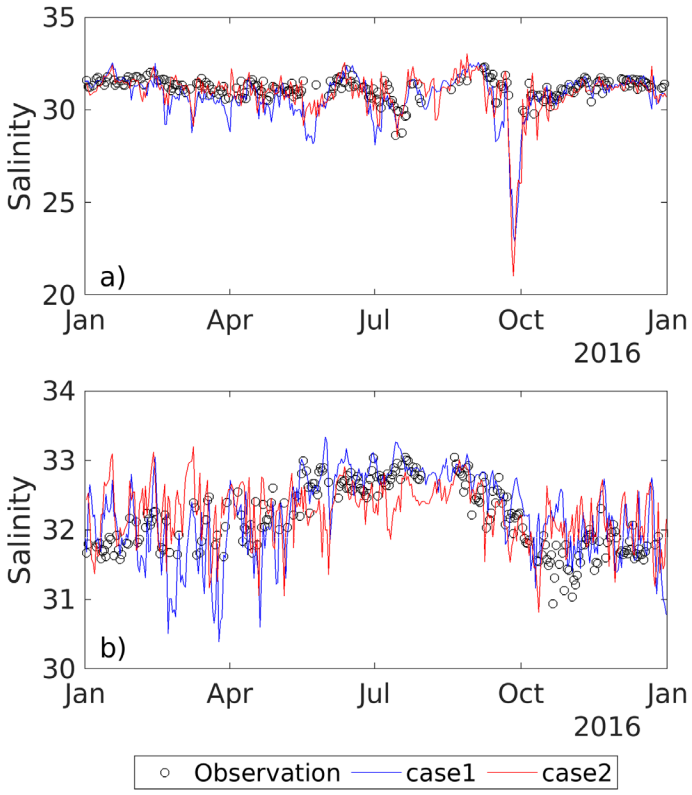

Figure 10. Timeseries of salinity at the No.3 buoy for observations, case 1, and case 2. a) water depth at 1.0 m; b) water depth at 12.0 m.

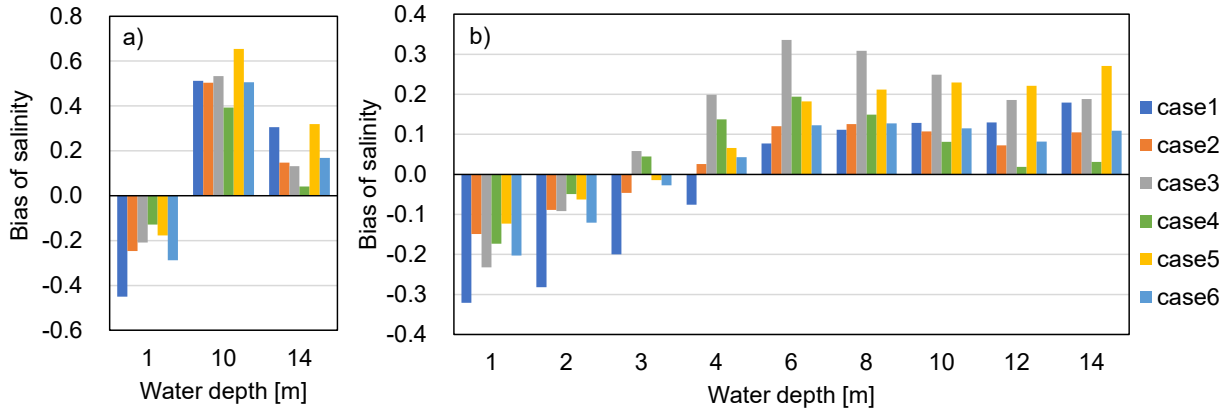

Figure 11. Bias between observed and modeled salinity for all experiments. a) Nakayama Channel; b) No.3 buoy.

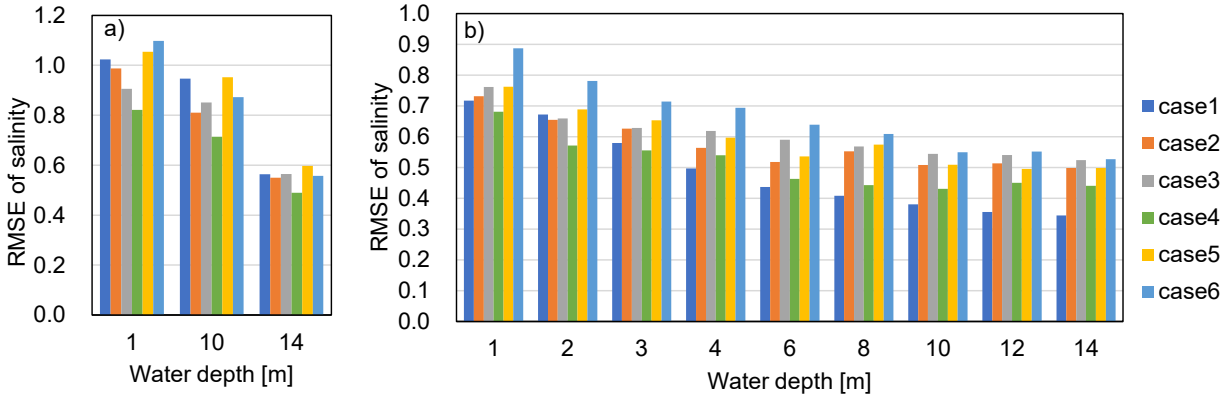

Figure 12. RMSE between observed and modeled salinity for all experiments. a) Nakayama Channel; b) No.3 buoy.

3.2 Effect of perturbations on boundary conditions

3.2.1 Atmospheric forcing

This subsection examines the effect of perturbation on atmospheric forcing on the data assimilation results. Compared to case 2, case 3, which does not perturb the air temperature and wind speed, does not improve the bias and RMSE values of water temperature in Nakayama Channel and at the No. 3 buoy (Figure **4** and Figure 5). This finding is particularly remarkable at the No. 3 buoy. Case 3 is the least improved among the data assimilation results (cases 2–6) for the bias and RMSE scores of both water temperature and SST (Figure 8). However, case 4, which perturbs the atmospheric forcing condition of air temperature, improves the water temperature from that of case 3 (Figure **4**, Figure 5, and Figure 8). Case 4 also exhibits better bias and RMSE scores than case 2 at a depth of −4 m or more at the No. 3 buoy, and better bias scores at a depth of −10 m or more in the Nakayama Channel. On the other hand, case 4 does not exhibit improvements from case 2 at the other depths, in the SST in Mikawa Bay on the east side

of Ise Bay (Figure 6 and Figure 7), or in the SST bias and RMSE scores (**Figure 8**). Therefore, the scores of case 2 are generally better than those of case 4. The ensemble spread of water temperature in the Nakayama Channel (Figure 13) is smaller in case 3 than in case 2, especially in the surface layer. Moreover, the ensemble spread of case 4 is larger than of case 3, but smaller than of case 2. At the No. 3 buoy (Figure 14), the ensemble spread of case 3 is even smaller than in the Nakayama Channel; thus, it is considered that the perturbation of air temperature and wind speed is a large error factor. Thus, perturbation of the atmospheric boundary conditions increases the ensemble spread of water temperature, especially near the surface layer, enabling effective assimilation of observed water temperature values.

For salinity (Figure 11 and Figure **12**), cases 3 and 4 exhibit similar bias and RMSE scores to case 2. However, at the No. 3 buoy (at a water depth of −4 m or more in Figure 11) and in the center of the bay (at a water depth of −10 m or less in Figure 15), the bias score is significantly worse. Therefore, it is considered preferable to perturb atmospheric forcing to avoid local salinity errors in the data assimilation. The difference in the ensemble spread of salinity is small between case 3 and case 4 (Figure 17 and Figure 18). In addition, the ensemble spread of cases 3 and 4 is smaller than of cases 5 and 6 (Figure 17 and Figure 18), particularly at the No. 3 buoy. These results indicate that, among the boundary conditions, wind speed has the greatest influence on the magnitude of the salinity ensemble spread and can be dominant depending on the location.

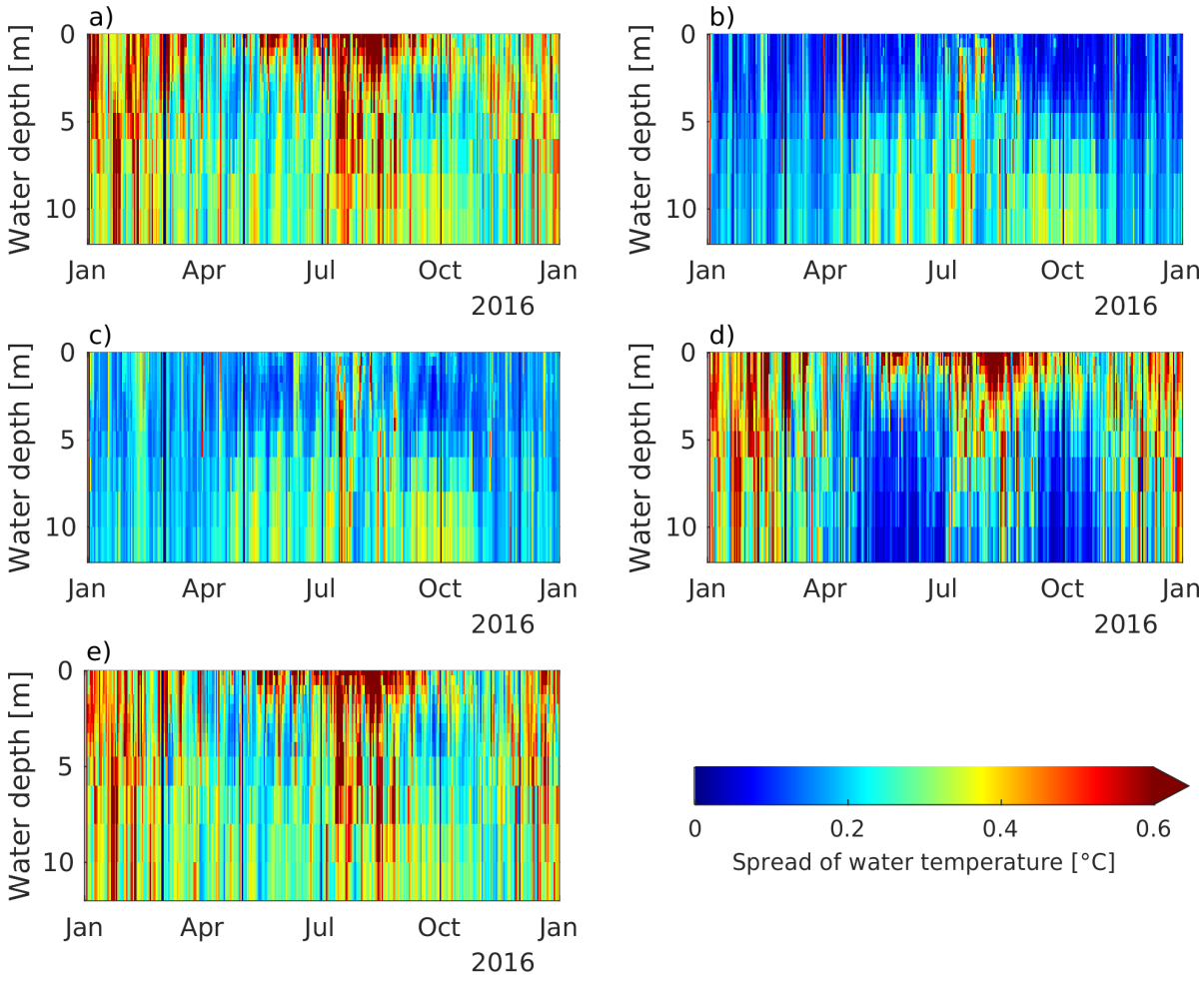

497

498 **Figure 13.** Temporal evolution of the ensemble spread of water temperature at Nakayama
499 Channel with water depth. a) Case 2, b) case 3, c) case 4, d) case 5, and e) case 6.
500

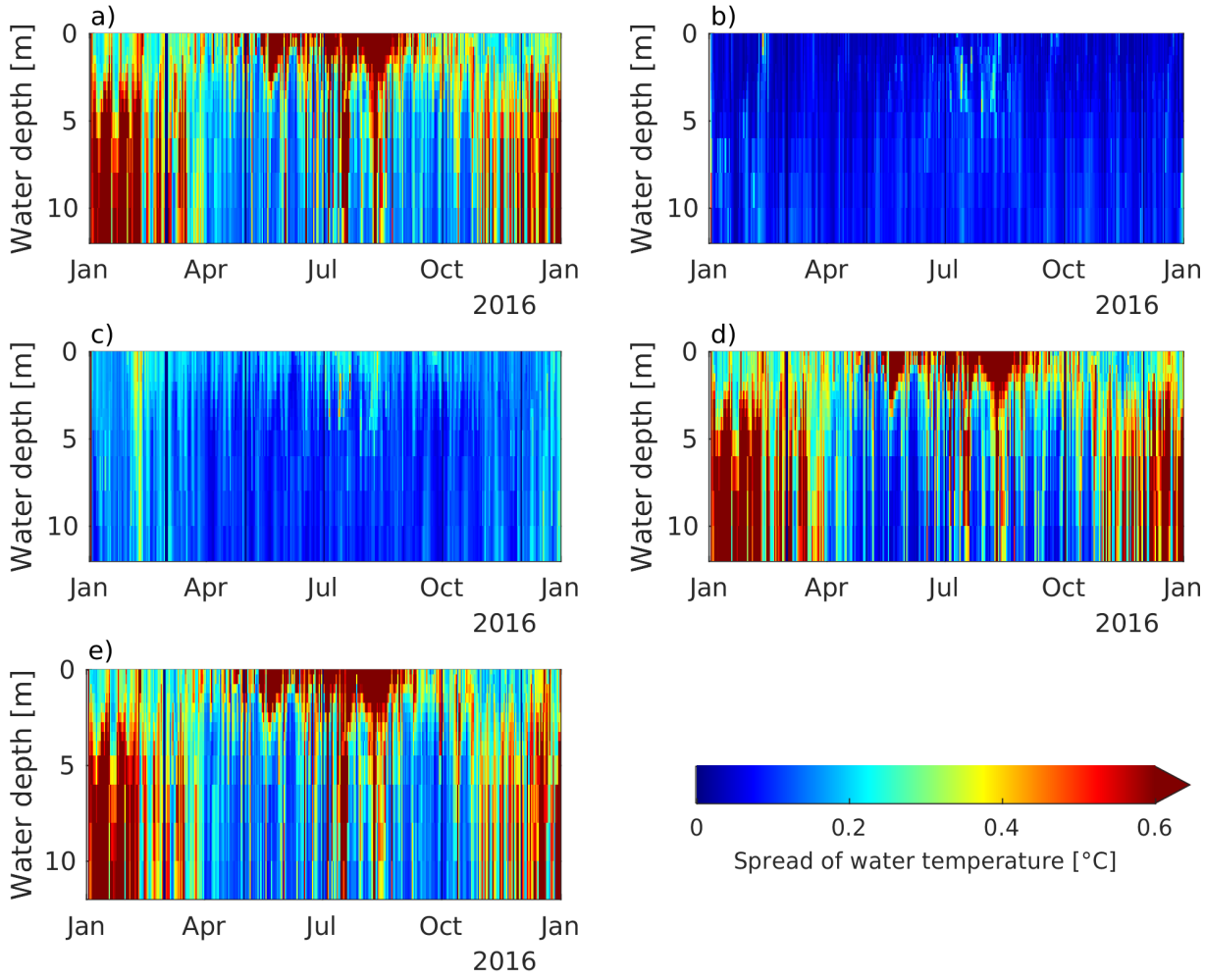

Figure 14. Temporal evolution of the ensemble spread of water temperature at the No. 3 buoy with water depth. a) Case 2, b) case 3, c) case 4, d) case 5, and e) case 6.

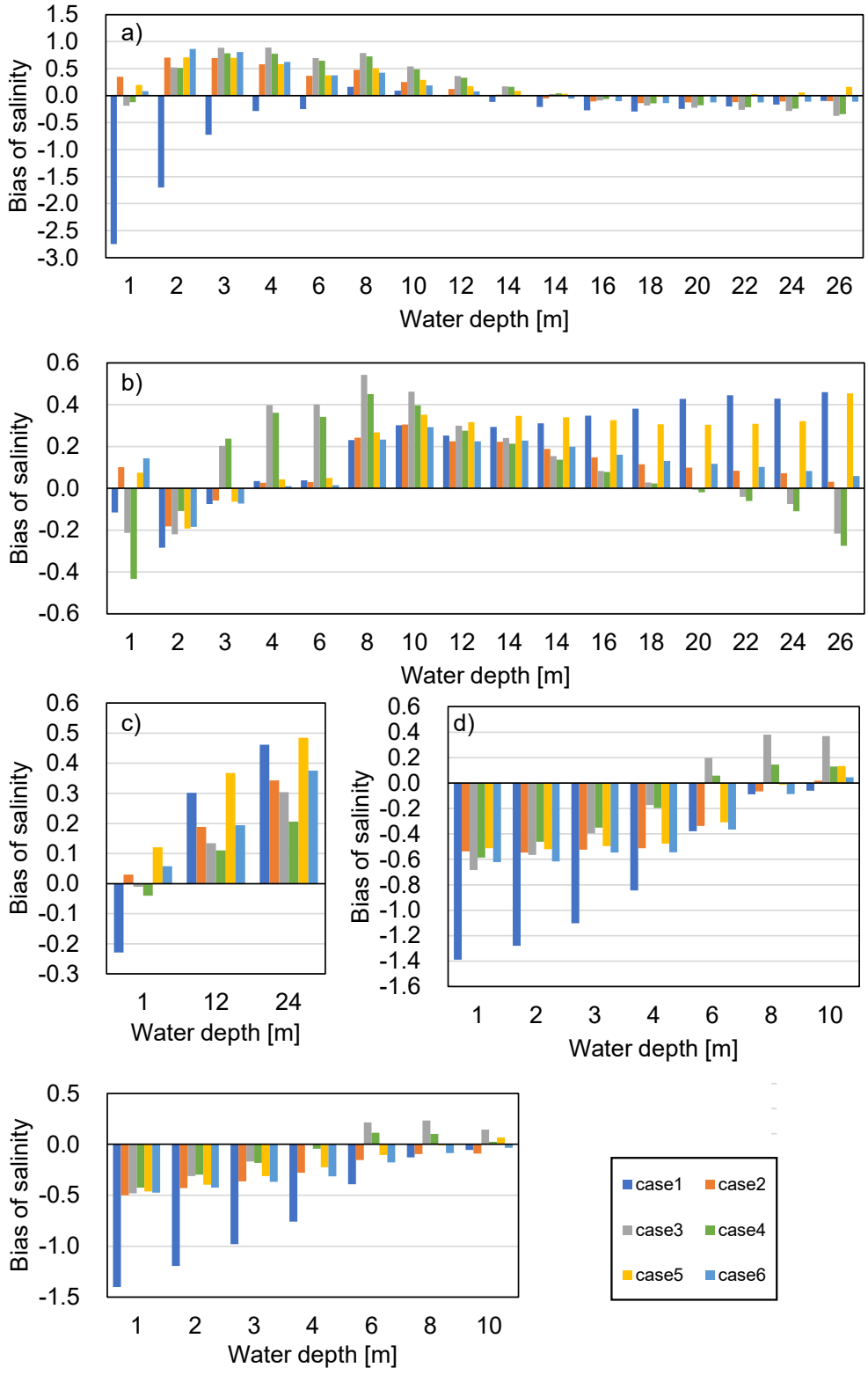

Figure 15. Bias of salinity between observations and model output using assimilated data from Table 2. a) Back of bay, b) center of bay, c) mouth of bay, d) No. 1 buoy, and e) No. 2 buoy.

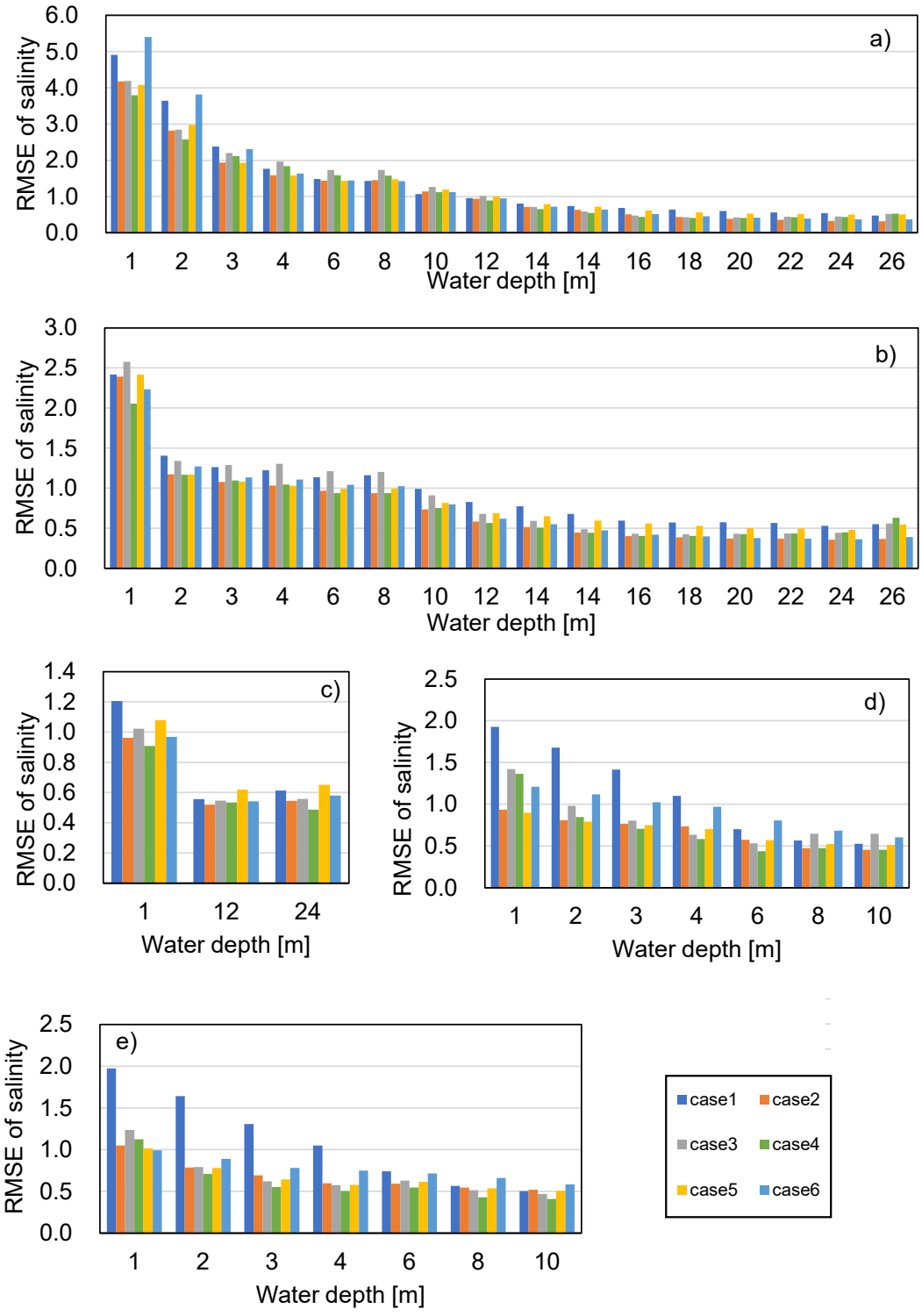

507

508 **Figure 16.** RMSE of salinity between observations and model output using assimilated data from
509 Table 2. a) Back of bay, b) center of bay, c) mouth of bay, d) No. 1 buoy, and e) No. 2 buoy.

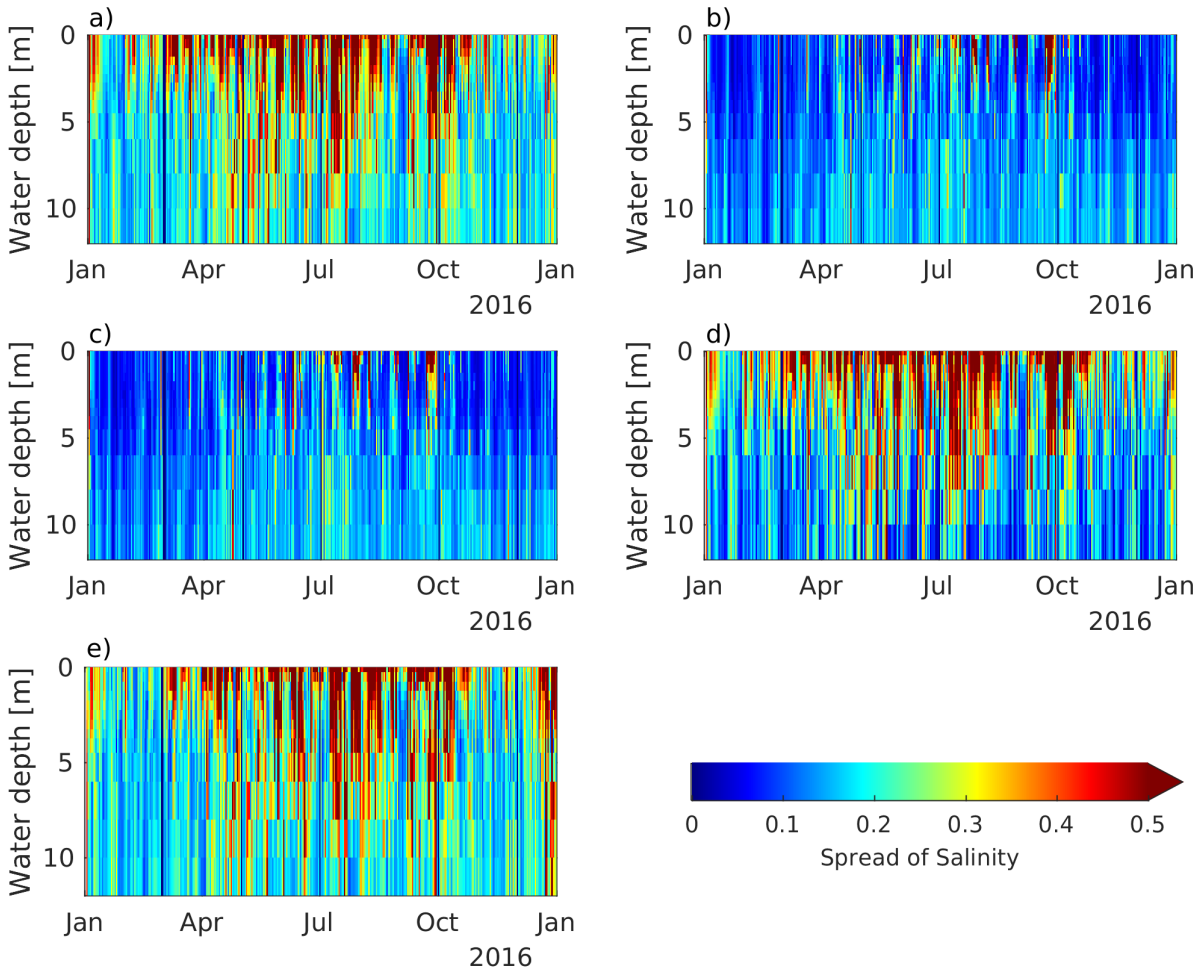

Figure 17. Temporal evolution of the ensemble spread of salinity at Nakayama Channel with water depth. a) Case 2, b) case 3, c) case 4, d) case 5, and e) case 6.

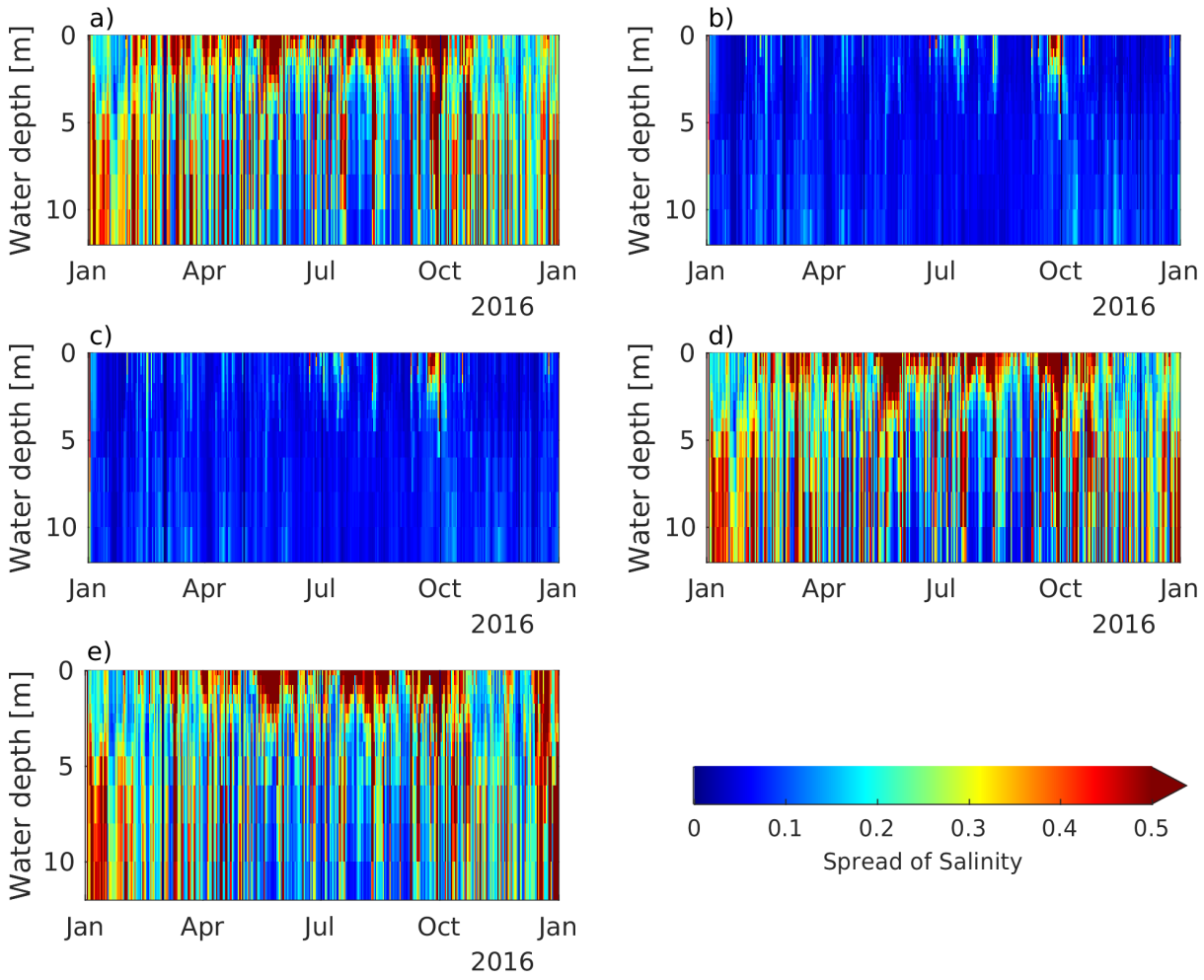

Figure 18. Temporal evolution of the ensemble spread of water temperature at the No. 3 buoy with water depth. a) Case 2, b) case 3, c) case 4, d) case 5, and e) case 6.

3.2.2 Lateral boundary conditions

This section examines the effect of perturbation to the lateral boundary conditions on the data assimilation results. In case 5, which does not perturb the lateral boundary conditions, the bias and RMSE scores of water temperature in Nakayama Channel and at the No. 3 buoy are not improved by data assimilation compared to those of case 2 (Figure **4** and Figure 5). This finding is particularly remarkable in the Nakayama Channel. Case 5 exhibits the least improvement in bias and RMSE scores among all data assimilation results (cases 2–6) in the Nakayama Channel and no improvement in SST scores around the bay mouth (Figure 6 and Figure 7). The ensemble spread of salinity is smaller for case 5 than for case 2 for all water depths in the Nakayama Channel (Figure 13). The large ensemble spread for case 5 from January to March and in December is thought to be because of perturbing the atmospheric boundary conditions because the ensemble spread for case 3 during the same period is small. However, at the No. 3 buoy, there is minimal difference in the ensemble spread between case 2 and case 5 (Figure 14).

Therefore, perturbation of the lateral boundary conditions increases the ensemble spread of water temperature at all water depths, especially near the bay mouth, and enables the effective assimilation of observed values.

Case 5 exhibits lower bias and RMSE scores for salinity than case 2 in the Nakayama Channel (Figure 11 and Figure **12**) and at the mouth of the bay (Figure 15 and Figure 16). The ensemble spread of salinity is smaller at the Nakayama Channel (Figure 17), which is similar to the results of water temperature. Again, there is almost no difference in the ensemble spread between case 2 and case 5 at the No. 3 buoy (Figure 18). Therefore, as with water temperature, perturbation of the lateral boundary conditions increases the ensemble spread at all water depths, especially near the bay mouth, and enables the effective assimilation of observed values.

3.2.3 River discharge forcing

Case 6, which does not perturb the river discharge forcing, shows a similar improvement in the bias and RMSE scores of water temperature from those of case 2 in Nakayama Channel and at the No. 3 buoy (Figure **4** and Figure 5). However, the bias and RMSE scores of SST are worse than those of case 2 in the inner part of the bay (Figure 6 and Figure 7). The ensemble spread of water temperature for case 6 and case 2 show similar trends in Nakayama Channel and at the No. 3 buoy. This result indicates that the effect of perturbing river discharge forcing is particularly large near the river mouth and decreases with distance from the river mouth. Therefore, perturbation of river discharge forcing ensures appropriate assimilation of water temperature data in the coastal estuary.

For salinity, the RMSE score of case 6 is worse than case 2 at the back of bay (Figure 16). Like water temperature, the error of the river boundary conditions has an increasing influence on salinity with proximity to the river mouth. Moreover, it is necessary to perturb river discharge forcing to improve the data assimilation results, especially near the river mouth.

4 Discussion

4.1 Performance and robustness of data assimilation

Previous studies have not examined the long-term applicability of regional data assimilation methods for coastal estuaries, nor their ability to reflect seasonal fluctuations. Moreover, although EnKF has been applied to OSSEs, before this study, it had not been applied to actual observation data from coastal areas. In this study, the proposed EnKF method achieved stable assimilation results for both water temperature (Figure 2 and Figure 3) and salinity (Figure 9 and Figure 10) throughout the year, and reflected seasonal fluctuations. Thus, the proposed regional data assimilation method for coastal estuaries exhibits good applicability and robustness. The assimilation of water temperature (Figure **4** and Figure 5) and salinity (Figure 11 and Figure **12**) data contributed to error correction in the vertical direction (i.e., with water depth). Water temperature was also corrected in the horizontal direction (**Figure 6** and **Figure 7**). This is because the error covariance was appropriately expressed by generating ensembles using the proposed method of perturbing boundary conditions.

4. 2 Effect of perturbations to boundary conditions

In comparison to the open ocean, lateral boundary conditions and river discharge forcing are relatively more important in a coastal estuary. However, due to inadequate observation data,

it is difficult to provide accurate boundary conditions, causing substantial errors in coastal numerical simulations. Therefore, in this study, a perturbation was applied to the three boundary conditions. Although the ensemble spread generally tends to degenerate in coastal estuary modeling, this was avoided by applying perturbations to lateral boundary conditions and river discharge forcing (Figure 13, Figure **14**, Figure **17**, and Figure **18**). Although perturbations are often applied to atmospheric forcing in ocean data assimilation methods, this is the first study to indicate the importance of applying perturbations to lateral boundary conditions and river discharge forcing in regional data assimilation for a coastal estuary.

In this study, the location where the perturbation was applied was examined, and the magnitude was obtained by error analyses through comparisons with observation data. According to the data assimilation results, the magnitude of perturbation was qualitatively appropriate. Therefore, the method of estimating the magnitude of the perturbation (*Appendix A)* is considered appropriate, and the error estimation method implemented in this study can be used for general purposes. However, this study did not evaluate the optimal magnitude of the perturbation; therefore, this should be considered in future work.

Vervatis et al. (2021) noted that, in the open ocean, perturbing the wind speed had the greatest effect on the ensemble spread of water temperature during data assimilation by EnKF, and that perturbation of other atmospheric forcing conditions (air temperature and sea level pressure) was less dominant. They also reported that wind uncertainty had a significant impact on upper ocean uncertainty for both the geostrophic and Ekman components defined by Sverdrup dynamics. Similarly, in our regional data assimilation for coastal estuaries, perturbation of the air temperature was also important for the ensemble spread of water temperature (**Figure 13**) besides wind speed. These results show the difference between open ocean and coastal modeling. Figure 4 (b) in Vervatis et al. (2021) shows that the ensemble spread caused by perturbation of the air temperature was large near the coastline (coastal area). Therefore, the effect of air temperature perturbations cannot be neglected during data assimilation in coastal areas.

4.3 Future work

The results here, are a crucial first step in regional coastal data assimilation; however, many issues remain unresolved. Specifically, the correlation of different boundary conditions was set to be small to avoid unintended accidental correlations. However, we could not confirm there were no problems with this setting. For example, the lateral boundary conditions of water temperature and salinity exhibit a certain correlation. Thus, it is necessary to verify the assimilation when the perturbation is applied according to the correlation obtained from observed values. Furthermore, the correlation coefficient between the discharge forcing of each river was set to 1, which is not the true value. Although the correlation for rivers with short distances between them is close to 1, rivers with long distances between them may require comparison of the observed river discharge and water temperatures to estimate the correlation coefficient.

Abundant observation data are obtained from satellite and in situ observations in coastal areas. However, the data assimilation method used in this study cannot simultaneously assimilate more observation data than ensemble members. Therefore, experiments with a greater amount of ensemble members are required to assimilate large amounts of observational data. Moreover, system error in this study was assumed to be constant, regardless of the time or season, and the perturbations (standard deviation ζ) of boundary conditions were set to constant values. Therefore, future research should examine whether the proposed data assimilation method is

suitable for detailed event analysis (e.g., strong winds, large-scale floods, water mass intrusion from the open ocean to the inner bay) where the model error, not the boundary conditions, has a significant effect.

Furthermore, confirmation of the reproducibility of salinity data was limited to a comparison of bias and RMSE scores using in situ observations, and the reproducibility of salinity distributions was not discussed. However, a method for calculating the highly accurate planar distribution of coastal areas using satellite observations has recently been developed (Nakada et al., 2018), which will be used to conduct salinity reproducibility analyses in future works.

Finally, instead of relying on data assimilation, it is also necessary to improve the simulation model. For example, the salinity bias is reversed between the surface and bottom layers in this study, which may be because the salinity of the model output is less diffused in the vertical direction than in reality. As the positive and negative biases are the same in the data assimilation results (Figure 11 and Figure 15), it is necessary to modify the simulation model to consider diffusion in the vertical direction.

4 Conclusions

Despite previous numerical experiments of data assimilation (OSSEs), this is the first study to apply the EnKF to regional data assimilation of coastal estuaries using actual long-term observation data. Specifically, data assimilation was performed for water temperature and salinity. According to comparisons with observation data not used in the assimilation, the simulated water temperature and salinity data were corrected in the horizontal and vertical directions (i.e., with water depth). In addition, the proposed method achieved stable long-term data assimilation over one year and responded to seasonal fluctuations. Besides perturbations to atmospheric forcing adopted in previous open ocean data assimilation, model accuracy scores, and the ensemble spread of water temperature and salinity revealed that perturbations of the lateral boundary conditions and river discharge forcing are important for regional data assimilation in coastal estuaries.

Acknowledgments

This study results from commissioned research from Chubu Regional Bureau, Ministry of Land, Infrastructure, Transport, and Tourism, Japan. This work was supported by JSPS KAKENHI Grant Number 21K14255. Observed data were obtained from Chubu Regional Bureau, Ministry of Land, Infrastructure, Transport, and Tourism of Japan, the Japan Meteorological Agency, Aichi Fisheries Research Institute, and the National Oceanic and Atmospheric Administration (NOAA). We extend thanks to Shun Ohishi and Teruhisa Okada for their advice on our study. We would like to thank Editage (www.editage.com) for the English language editing. No potential conflict of interest was reported by the authors.

References

Anderson, J. L., & Anderson, S. L. (1999). A Monte Carlo implementation of the nonlinear filtering problem to produce ensemble assimilations and forecasts. *Monthly Weather Review*, *127*(12), 2741–2758. https://doi.org/10.1175/1520-0493(1999)127<2741:AMCIOT>2.0.CO;2

Baduru, B., Paul, B., Banerjee, D. S., Sanikommu, S., & Paul, A. (2019). Ensemble based regional ocean data assimilation system for the Indian Ocean: Implementation and evaluation. *Ocean Modelling*, *143*. https://doi.org/10.1016/j.ocemod.2019.101470

Bougeault, P., Toth, Z., Bishop, C., Brown, B., Burridge, D., Chen, D. H., et al. (2010). The THORPEX Interactive Grand Global Ensemble. *Bulletin of the American Meteorological Society*, *91*(8), 1059–1072. https://doi.org/10.1175/2010BAMS2853.1

Brankart, J.-M., Candille, G., Garnier, F., Calone, C., Melet, A., Bouttier, P.-A., et al. (2015). A generic approach to explicit simulation of uncertainty in the NEMO ocean model. *Geoscientific Model Development*, *8*(5), 1285–1297. https://doi.org/10.5194/gmd-8-1285-2015

Edwards, C. A., Moore, A. M., Hoteit, I., & Cornuelle, B. D. (2015). Regional ocean data assimilation. *Annual Review of Marine Science*, *7*(1), 21–42. https://doi.org/10.1146/annurev-marine-010814-015821

Evensen, G. (1994). Sequential data assimilation with a nonlinear quasi-geostrophic model using Monte Carlo methods to forecast error statistics. *Journal of Geophysical Research*, *99*(C5), 10143. https://doi.org/10.1029/94JC00572

Evensen, G. (2003). The Ensemble Kalman Filter: theoretical formulation and practical implementation. *Ocean Dynamics*, *53*(4), 343–367. https://doi.org/10.1007/s10236-003-0036-9

Evensen, G. (2009). *Data assimilation: the Ensemble Kalman Filter* (2. ed). Dordrecht: Springer.

Fisher, M., & Courtier, P. (1995). Estimating the covariance matrices of analysis and forecast error in variational data assimilation. ECMWF Technical Memoranda, 220. https://doi.org/10.21957/1DXRASJIT

Fisher, R. A., & Yates, Frank. (1948). *Statistical tables for biological, agricultural and medical research*. London: Oliver and Boyd.

Fu, L.-L., Fukumori, I., & Miller, R. N. (1993). Fitting dynamic models to the geosat sea level observations in the Tropical Pacific Ocean. Part II: A linear, wind-driven model. *Journal of Physical Oceanography*, *23*(10), 2162–2181. https://doi.org/10.1175/1520-0485(1993)023<2162:FDMTTG>2.0.CO;2

Gaspari, G., & Cohn, S. E. (1999). Construction of correlation functions in two and three dimensions. *Quarterly Journal of the Royal Meteorological Society*, *125*(554), 723–757. https://doi.org/10.1002/qj.49712555417

Hafeez, M. A., Nakamura, Y., Suzuki, T., Inoue, T., Matsuzaki, Y., Wang, K., & Moiz, A. (2021). Integration of Weather Research and Forecasting (WRF) model with regional coastal ecosystem model to simulate the hypoxic conditions. *Science of The Total Environment*, *771*, 145290. https://doi.org/10.1016/j.scitotenv.2021.145290

Hamill, T. M., Whitaker, J. S., & Snyder, C. (2001). Distance-Dependent Filtering of Background Error Covariance Estimates in an Ensemble Kalman Filter. *Monthly Weather Review*, *129*(11), 2776–2790. https://doi.org/10.1175/1520-0493(2001)129<2776:DDFOBE>2.0.CO;2

Henderson-Sellers, B. (1985). New formulation of eddy diffusion thermocline models. *Applied Mathematical Modelling*, *9*(6), 441–446. https://doi.org/10.1016/0307-904X(85)90110-6

Hoffman, M. J., Miyoshi, T., Haine, T. W. N., Ide, K., Brown, C. W., & Murtugudde, R. (2012). An advanced data assimilation system for the Chesapeake Bay: Performance evaluation. *Journal of Atmospheric and Oceanic Technology*, *29*(10), 1542–1557. https://doi.org/10.1175/JTECH-D-11-00126.1

https://doi.org/10.1175/JTECH-D-11-00126.1

Hoteit, I., Luo, X., Bocquet, M., Köhl, A., & Ait-El-Fquih, B. (2018). Data assimilation in oceanography: Current status and new directions. In E. P. Chassignet, A. Pascual, J. Tintoré, & J. Verron (Eds.), *New Frontiers in Operational Oceanography*. GODAE OceanView. https://doi.org/10.17125/gov2018.ch17

Khanarmuei, M., Mardani, N., Suara, K., Sumihar, J., Sidle, R. C., McCallum, A., & Brown, R. J. (2021). Assessment of an ensemble-based data assimilation system for a shallow estuary. *Estuarine, Coastal and Shelf Science*, *257*. https://doi.org/10.1016/j.ecss.2021.107389

Kunii, M., & Miyoshi, T. (2012). Including Uncertainties of Sea Surface Temperature in an Ensemble Kalman Filter: A Case Study of Typhoon Sinlaku (2008). *Weather and Forecasting*, *27*(6), 1586–1597. https://doi.org/10.1175/WAF-D-11-00136.1

Kuwagata, T., & Kondo, J. (1990). Estimation of aerodynamic roughness at the regional meteorological stations (AMeDAS) in the central part of Japan. *TENKI*, *37*(3), 55–59.

Kwon, K. M., Choi, B.-J., Lee, S.-H., Kim, Y. H., Seo, G.-H., & Cho, Y.-K. (2016). Effect of model error representation in the Yellow and East China Sea modeling system based on the ensemble Kalman filter. *Ocean Dynamics*, *66*(2), 263–283. https://doi.org/10.1007/s10236-015-0909-8

Lima, L. N., Pezzi, L. P., Penny, S. G., & Tanajura, C. A. S. (2019). An investigation of ocean model uncertainties through ensemble forecast experiments in the Southwest Atlantic Ocean. *Journal of Geophysical Research: Oceans*, *124*(1), 432–452. https://doi.org/10.1029/2018JC013919

Matsuzaki, Y., & Inoue, T. (2020). A Study of Calculation Conditions of Data Assimilation for Flow Analysis of Closed Waters by Ensemble Kalman Filter. *Technical Note of the Port and Airport Research Institute*, (1367), 35.

Matsuzaki, Y., Fujiki, T., Kawaguchi, K., Inoue, T., & Iwamoto, T. (2021). Application of the WRF model to the coastal area at Ise Bay, Japan: evaluation of model output sensitivity to input data. *Coastal Engineering Journal*, *63*(1), 17–31. https://doi.org/10.1080/21664250.2020.1830485

Mirouze, I., & Storto, A. (2019). Generating atmospheric forcing perturbations for an ocean data assimilation ensemble. *Tellus A: Dynamic Meteorology and Oceanography*, *71*(1), 1624459. https://doi.org/10.1080/16000870.2019.1624459

Moore, A. M., Arango, H. G., Broquet, G., Powell, B. S., Weaver, A. T., & Zavala-Garay, J. (2011). The Regional Ocean Modeling System (ROMS) 4-dimensional variational data assimilation systems. *Progress in Oceanography*, *91*(1), 34–49. https://doi.org/10.1016/j.pocean.2011.05.004

Nakada, S., Kobayashi, S., Hayashi, M., Ishizaka, J., Akiyama, S., Fuchi, M., & Nakajima, M. (2018). High-resolution surface salinity maps in coastal oceans based on geostationary ocean color images: quantitative analysis of river plume dynamics. *Journal of Oceanography*, *74*(3), 287–304. https://doi.org/10.1007/s10872-017-0459-4

Nakamura, Y., & Hayakawa, N. (1991). Modelling of thermal stratification in lakes and coastal seas (pp. 227–236). Presented at the IAHS Publication (International Association of Hydrological Sciences). Retrieved from https://www.scopus.com/inward/record.uri?eid=2-s2.0-0025843997&partnerID=40&md5=7952862f01733aee89cce203e30718ca

Nimiya, H., Akasaka, H., & Matsuo, Y. (1996). A method to estimate the hourly downward atmospheric radiation using AMeDAS data. *The Society of Heating, Air-Conditioning Sanitary Engineers of Japan*, (60), 133–144.

Nimiya, H., Akasaka, H., Matsuo, Y., & Soga, K. (1997). A method to estimate the hourly solar radiation using AMeDAS data Part2-Application to the improved sunshine recorder of AMeDAS. *The Society of Heating, Air-Conditioning Sanitary Engineers of Japan*, (65), 53–65.

Orlanski, I. (1976). A simple boundary condition for unbounded hyperbolic flows. *Journal of Computational Physics*, *21*(3), 251–269. https://doi.org/10.1016/0021-9991(76)90023-1

Penny, S. G., Behringer, D. W., Carton, J. A., & Kalnay, E. (2015). A hybrid global ocean data assimilation system at NCEP. *Monthly Weather Review*, *143*(11), 4660–4677. https://doi.org/10.1175/MWR-D-14-00376.1

Prasad, R. (1967). A nonlinear hydrologic system response model. *Journal of the Hydraulics Division*, *93*(4), 201–222.

Sakov, P., Counillon, F., Bertino, L., Lisæter, K. A., Oke, P. R., & Korablev, A. (2012). TOPAZ4: an ocean-sea ice data assimilation system for the North Atlantic and Arctic. *Ocean Science*, *8*(4), 633–656. https://doi.org/10.5194/os-8-633-2012

Sanikommu, S., Toye, H., Zhan, P., Langodan, S., Krokos, G., Knio, O., & Hoteit, I. (2020). Impact of atmospheric and model physics perturbations on a high-resolution ensemble data assimilation system of the Red Sea. *Journal of Geophysical Research: Oceans*, *125*(8). https://doi.org/10.1029/2019JC015611

Stanev, E. V., Schulz-Stellenfleth, J., Staneva, J., Grayek, S., Grashorn, S., Behrens, A., et al. (2016). Ocean forecasting for the German Bight: from regional to coastal scales. *Ocean Science*, *12*(5), 1105–1136. https://doi.org/10.5194/os-12-1105-2016

Tanaka, Y., & Suzuki, K. (2010). Development of Non-Hydrostatic Numerical Model for Stratified Flow and Upwelling in Estuary and Coastal Areas. *Report of the Port and Airport Research Institute*, *49*(1), 3–26.

Turner, M., Walker, J., & Oke, P. (2008). Ensemble member generation for sequential data assimilation. *Remote Sensing of Environment*, *112*(4), 1421–1433. https://doi.org/10.1016/j.rse.2007.02.042

Vandenbulcke, L., & Barth, A. (2015). A stochastic operational forecasting system of the Black Sea: Technique and validation. *Ocean Modelling*, *93*, 7–21. https://doi.org/10.1016/j.ocemod.2015.07.010

Vervatis, V. D., De Mey-Frémaux, P., Ayoub, N., Karagiorgos, J., Ghantous, M., Kailas, M., et al. (2021). Assessment of a regional physical–biogeochemical stochastic ocean model. Part 1: Ensemble generation. *Ocean Modelling*, *160*. https://doi.org/10.1016/j.ocemod.2021.101781

Weaver, A., & Courtier, P. (2001). Correlation modelling on the sphere using a generalized diffusion equation. *Quarterly Journal of the Royal Meteorological Society*, *127*(575), 1815–1846. https://doi.org/10.1002/qj.49712757518

Whitaker, J. S., & Hamill, T. M. (2012). Evaluating methods to account for system errors in ensemble data assimilation. *Monthly Weather Review*, 140(9), 3078–3089. https://doi.org/10.1175/MWR-D-11-00276.1

World Meteorological Organization. (2008). *Guide to meteorological instruments and methods of observation.* Geneva, Switzerland: World Meteorological Organization.

Appendix

A. Estimation of the magnitude of perturbation to boundary conditions

A.1 Air temperature

The dominant error factors of the atmospheric forcing condition of air temperature were the differences between observation points (sea and ground) and the influence of spatial interpolation. Therefore, it is assumed that the air temperatures are accurate at five locations in Ise Bay (center of the bay, mouth of the bay, and buoys 1 to 3), where the observed air temperature is shown in **Table 2**, and from April 2015 to December 2019. The boundary condition between the air temperature observed at the monitoring locations in Ise Bay and the air temperature calculated at the same position was extracted every hour. The cumulative frequency distribution of the absolute difference between the observed value and the calculated value was obtained after subtracting the average error, and the temperature at which the cumulative frequency was 68.2% was calculated as 3.05 °C. Therefore, we added system noise with a normal distribution and a standard deviation of the ξ value of 3.05 °C to the boundary conditions of air temperature for each ensemble member.

A.2 Wind speed

The error factor and ξ of the atmospheric forcing condition of wind speed was estimated using the same method as that for air temperature. The cumulative frequency distribution of the absolute difference between the observed value and the boundary condition was obtained, and the value at which the cumulative frequency was 68.2% was calculated as 3.45 m s^{-1}. Therefore, we added system noise with a normal distribution and a standard deviation of the ξ value of 3.45 m s^{-1} to the boundary conditions of wind speed for each ensemble member.

A.3 Water temperature of the lateral boundary

The error factor of the lateral boundary condition of water temperature was mainly caused because the original data used to create the boundary conditions was not observed during the simulation period, but was the average value over 10 years, as explained in section 2.2. Then, ξ was estimated as follows. First, it was assumed that the observed water temperature is accurate. Second, the error was estimated by comparing the observed values with the open boundary conditions. The comparison period was for one year (2015). The cumulative frequency distribution of the absolute difference between the observed value and the boundary condition was calculated after subtracting the average error, and the value at which the cumulative frequency was 68.2% was calculated as 0.73 °C. Therefore, we added system noise with a normal distribution and a standard deviation of the ξ value of 0.73 °C to the open boundary condition of water temperature for each ensemble member.

A.4 Salinity of the lateral boundary

The error factor and ξ of the lateral boundary condition of salinity was estimated using the same method as that for water temperature. The cumulative frequency distribution of the absolute difference between the observed value and the boundary condition was obtained, and the value at which the cumulative frequency was 68.2% was calculated as 0.20. Therefore, we

added system noise with a normal distribution and a standard deviation of the ξ value of 0.20 to the boundary conditions of salinity for each ensemble member.

A.5 River discharge

The error factors of river discharge were predominantly the estimation error of the storage function method and the spatiotemporal error of input precipitation. Thus, the ξ value of river discharge was estimated as follows. It was assumed that the rate of fluctuation inherent in river discharge is the same for each river simultaneously. When the rate of discharge fluctuation varies for each river, the variation is regarded as the error of the river discharge. The analysis period was set from April 2015 to December 2019, and the average discharge was calculated for the 10 major rivers flowing into Ise Bay. The river discharge change rate was calculated by dividing the discharge of each river at each time by the average discharge for each river, and the standard deviation for each time was obtained. When the cumulative frequency of the standard deviation was 68.2%, the value was calculated as 0.35. Therefore, the boundary condition was multiplied by the system noise with a normal distribution and a standard deviation of 0.35.

A.6 River water temperature

The spatial correlation error and estimation error were considered the dominant error factors of river water temperature. Therefore, when there was a difference in water temperature between rivers, system noise was added by assuming that it was an error. The standard deviation regarding the variation in water temperature at each time for each river was calculated for the 10 major rivers that flow into Ise Bay. The analysis period was from April 2015 to December 2019. Then, if the distribution of the magnitude of the error for the entire period follows a normal distribution, the cumulative frequency distribution was created, and the value at which the cumulative frequency was 68.2% was calculated. Therefore, we added system noise with a normal distribution and a standard deviation of the ξ value of 1.21 °C to the boundary condition of temperature for each ensemble member.